DEPOSITIONAL SYSTEMS INTERPRETATION OF EARLY PERMIAN MIXED SILICICLASTICS AND CARBONATES, MIDLAND BASIN, TEXAS

Robert Murphy

Submitted to the faculty of the University Graduate School
in partial fulfillment of the requirements for the degree
Master of Sciences
in the Department of Geological Sciences
Indiana University
February 2015

Accepted by the Graduate Faculty, Indiana University, in partial fulfillment of the requirements for the degree of Master of Science in Geological Sciences.

Master's Thesis Committee

Juergen Schieber, Ph.D., Chair

Abhijit Basu, Ph.D.

John Rupp

Acknowledgements

I wish to thank the following for their guidance and support:

Dr. Juergen Schieber

Abhijit Basu

John Rupp

Brian Keith

Indiana University Shale Research Lab

Indiana University Department of Geological Sciences

Indiana Geological Survey

Pioneer Natural Resources Company

Robert Murphy

DEPOSITIONAL SYSTEMS INTERPRETATION OF EARLY PERMIAN MIXED SILICICLASTICS AND CARBONATES, MIDLAND BASIN, TEXAS

In this study, a core from the Midland basin of West Texas was examined in detail to determine the depositional setting of an Upper Wolfcampian and Lower Leonardian-aged mudstone succession. The studied sediments were deposited close to the center of the Midland Basin in a deep water, mixed carbonate and siliciclastic system. Core X was described on a centimeter scale and lithofacies were defined on the basis of mineralogy, texture, sedimentary structure, and degree of bioturbation. Their main features are summarized from bottom to top of the cored interval. The Wolfcamp B2 and B1 intervals consist of multiple facies types, but are dominated by organic rich silty mudstone, skeletal argillaceous packstone, and bioclast-lithoclast floatstone. The Wolfcamp A3 and A2 intervals are dominated by fine grained, resedimented carbonates in the form of grainstone beds that grade upward into packstone and mudstone. Structures attributed to post depositional slumping are common. The Wolfcamp A1 interval consists of thin grainstone beds and thick sections of interbedded silty mudstone and muddy siltstone. The Dean Formation overlies the Wolfcamp interval and consists of thick beds of very fine grained, well cemented, sandstone and muddy siltstone. Of the described facies, the clay and silt rich varieties are interpreted as hemipelagic sediments deposited by suspension settling, bottom currents, or

dilute density flows. In contrast, carbonate rich facies are interpreted as deposited by a spectrum of sediment gravity flow processes. Moderate to high levels of bioturbation in all clay and silt rich facies suggests dysoxic to suboxic conditions within the basin during the time of deposition.

An SEM investigation of pore types and their distribution led to the recognition of three pore types: phyllosilicate framework pores, organic matter pores, and dissolution pores. SEM observations and conventional core analysis indicate that the greatest porosity occurs in the clay and silt rich facies, whereas grainstones and cemented sandstones are the least porous.

Rock Eval pyrolysis data were integrated with the core description to help identify the most organic rich facies. Clay and silt rich facies show the highest average TOC, whereas the grainstone facies show the lowest average TOC values.

Table of Contents

List of Figures

List of Tables

Introduction

The Midland Basin is a sub-basin in the broader Permian Basin region of west Texas. The region has been a major oil producing province for over 90 years and in recent time has seen a great resurgence in drilling activity. At the turn of the century only 30% of the estimated original oil in place had been produced (Dutton et al., 2005). During the last two decades, technological advancements in reservoir development practices such as directional drilling and hydraulic fracturing have led to improved recovery from existing fields and a renewed interest in formations previously thought to be unproductive. Two such examples are the sequences of fine-grained clastic and interbedded carbonate rocks of the lower Permian-aged Wolfcamp and Lower Leonard in the southern Midland Basin. These rocks blanket much of the basin, were deposited in the deeper portions of the basin, and contain abundant organic matter. They are considered to be the source rocks for many of the conventional reservoirs found in the basin.

The Permian basin as a whole is one of the major oil producing regions in the world and as a result has been the subject of a great number of geologic studies, the objective of which has been to establish the age, stratigraphy, depositional facies, and regional setting of the hydrocarbon bearing strata. Other studies of the basin were concerned with developing exploration methods, drilling practices, and completion techniques (Atchley et al., 1999; Montgomary, 1996; Dutton et al., 2003; Hamlin and Baumgardner, 2012; Ward et al., 1986). Until the mid-1980's most research regarding the Midland Basin had been focused on

interpreting the depositional environments and associated petrophysical characteristics of the shallow platform and slope detrital carbonate facies. Renewed interest in late Paleozoic strata, driven in part by high oil prices, led to new studies in which the deep-water resedimented carbonates and hemipelagic mudstones were examined. This report incorporates well-established interpretations of the regional depositional setting and stratigraphy with observations made on a core that spans the interval from the upper Wolfcamp to the Lower Spraberry. Silver and Todd (1969) detailed the geologic processes, depositional setting, and cyclic development that characterize the Northern Delaware and Midland basins. Hanford (1981) described the sedimentology, genetic stratigraphy, and depositional processes of the Dean and Spraberry Formations from the northern platform to the central basin. Hobson et al. (1985) described lithofacies and depositional settings of the Late Pennsylvanian and Early Permian deep-water deposits in the southern part of Midland Basin. S.J. Mazzullo has published numerous papers over the last 30 years on the shore to basin facies development of Early Permian strata (Mazzullo, S.J., 1979,1980, 1981,1982,1995,1997,1998, 2004; Mazzullo and Harris, 1991; Mazzullo and Reid, 1989). Mazzullo and Reid, (1989) relate the evolutionary development of depositional systems within Lower Permian platform and basin sequences on the North Platform to such parameters as relative sea-level fluctuations, history of basin subsidence, variations in sedimentation rates, and the effects on sequence development of contrasting patterns of carbonate and siliciclastic sedimentation. Hamlin and Baumgardner (2012), provide an excellent summary of Wolfcampian

and Leonardian stratigraphy, depositional systems, and reservoir development within the Midland Basin.

Much of the examined core is composed of medium to thin beds (beds less than 10” thick) of mixed siliciclastic and carbonate sediments that are below the resolution of standard geophysical logging tools. Geophysical well logs, while providing important information about formation properties, fail to fully capture the heterogeneity of fine-grained, thinly bedded formations. Logging tools measure a signal that is a mixture of the combined properties of the beds within the vertical resolution of the tool. Logging tool detection limits, influenced by bed thickness and the contrast between neighboring beds, prohibit the direct identification of thin beds or the direct measurement of the physical properties of individual thin beds. An effective way to directly characterize fine grained**,** thin-bedded rocks is to describe a core at a series of scales that makes use of slabbed core, core photos, thin sections, and argon ion milled SEM samples. A core description that includes compositional variation, bed and lamina thicknesses, depositional and diagenetic textures, bedding contacts, grain-size variability, and depositional processes informs our understanding of how sediment transport, deposition, and diagenesis interact to produce the individual rock types that we observe. The resultant detailed, multi-scale description of the core can then be integrated with data from x-ray diffraction, Rock-Eval pyrolysis, and porosity and permeability measurements to support well log analyses. High-resolution gamma ray measurements are commonly collected on core and can be useful in calibrating the core to the well logs.

The combined data sets provide information that enhances our understanding of the complex relationship between lithology, depositional setting, organic richness, and the resultant porosity, and permeability distributions. Although the study of a single core, no matter how detailed, can only provide a snapshot of the various depositional conditions and processes that combined to create a vertical succession of facies, it nonetheless provides a good stepping off point to systematically extend such findings to the surrounding region in order to determine the controls on large-scale temporal and spatial facies variability. This information can then be applied to exploration and production operations by helping to identify, characterize, and predict the location of drilling prospects.

Regional Setting

The Late Pennsylvanian to Middle Permian paleogeography of the Permian basin was defined by tectonic modification of the ancestral Tobosa Basin, a broad, shallow, tectonic sag located between the Texas Arch to the west and the Diablo Platform to the east (Figure 1) (Frenzel, H.N., 1988). Following a long period of relative stability during the early Paleozoic, the southern margin of the North American craton was subjected to increasing tectonic activity that re-shaped the Tobosa basin into a series of multiple sub-basins separated by structural uplifts (Figure 1). This period of heightened tectonism lasted from the Late Mississippian to Early Permian and culminated in the Marathon-Ouachita Orogeny of early Pennsylvanian time. Along the Ouachita-Marathon margin, collisional convergence of the North American craton and Gondwana reactivated pre-existing high angle to vertical fault systems and created massive clastic wedge aprons that invaded rapidly subsiding foreland basins, (Sloss, L.L., 1988). The Marathon allochthon formed a highland that effectively created the southern boundary of the Permian Basin region (Figures 1 and 15) (Ross, 1986).

Following the period of maximum compressional tectonism during the Early Pennsylvanian, the newly formed Delaware and Midland Basins, separated by a intervening high, underwent rapid subsidence that produced extensive asymmetrical troughs with the deepest part of the basins being closer to the Central Basin platform than the surrounding Northern or Eastern Shelves (Adams, J.E., 1965). By Early Permian time, carbonate environments had

developed on the Central Basin platform and surrounding shallow shelf areas, leading to the growth of massive limestone build-ups behind which lagoons and sabkhas developed.

The key paleo-geographic features that influence the depositional character of the basin are shown in Figure1. The core portion of the Permian Basin was a structural sag consisting of the Midland Basin to the east and the deeper Delaware Basin to the west. The Central Basin platform separated the Delaware Basin from the Midland Basin and was the site of significant carbonate shelf deposition. In the northern part of the Permian Basin the San Simon Channel separated the Central Basin Platform from the Northwestern shelf. In the southern part of the basin the Sheffield Channel separated the southern margin of the Midland Basin from the southern shelf. The Eastern and Northern Platforms of the Midland Basin are composed of a depositional complex that records cyclic platform to basin sequences of alternating carbonate and terrigenous clastic beds (Silver and Todd, 1969). During Early Permian time the Midland Basin was an actively subsiding depocenter in which platform deposits (carbonate, evaporites, and shale) surrounded deep basins with mixed carbonate and siliciclastic input (Adams, 1965; Silver and Todd, 1969; Ross, 1986; Yancey, 1991).

Midland Basin Stratigraphy

The stratigraphy of the Midland Basin is well established due to a long history of geologic fieldwork and research related to petroleum exploration that utilized outcrop studies, core studies, well log data, and seismic data. This comprehensive understanding of basin development, regional framework, and platform to basin changes in lithology is key to recognizing the significance of vertical changes in mineralogy and sedimentary structures observed in the core. Historically, the Northern Platform of the Midland basin has been given the most attention with regard to correlating cyclic shelf carbonates to mixed siliciclastic and detrital carbonates deposited in the basin. The depositional framework of the Northern Platform is grossly similar to that of the Eastern Shelf of the southern Midland Basin, thereby providing a valuable analog for understanding stratigraphy, sedimentology, and facies development (Mazzullo and Reid, 1989).

The drill core examined in this study covers a continuous stratigraphic sequence within Lower Permian strata of the Upper Wolfcampian Series and extends through the Lower Spraberry Formation of the Upper Leonardian Series. Stratigraphic relationships for the study area and its relation to the Northern Shelf, Eastern Shelf and Central Basin Platform are shown in Figure 2. The earliest geologic descriptions did not subdivide the Wolfcampian or Lower Leonardian Series rocks and shelf to basin correlations were difficult due to the complex nature of the mixed carbonate and siliciclastic sediments (Hobson et al., 1985; Montgomery, 1996). However, later studies, based on fusulinid zonation,

made it possible to subdivide both Series into component bio-stratigraphic and lithic units that are recognizable on logs and seismic lines throughout the Permian Basin (Mazzullo and Reid, 1989). The location of the biostratigraphic boundary between the Upper Wolfcamp and Lower Leonard has been redefined several times, and has led to some confusion in naming conventions. Based on detailed regional fusulinid studies (Reid et al., 1988), those rocks that were previously thought to be the latest Upper Wolfcampian in age are now known to be the Lower Leonardian basinal equivalent of the Wichita and Lower Clear Fork Formations found on the shelf. In this study, the Wolfcamp A3, A2, and A1 name designations are used for the Lower Leonardian aged intervals.

Methodology

The focus of this study is the examination of a single, continuous length of drill core measuring 729 feet. Core X was recovered from a well in northern Reagan County, Texas. The core spans a measured depth of 8,148 feet to 8,877 feet. The stratigraphic intervals represented include, from oldest to youngest, the upper Wolfcampian (Wolfcamp B2, B1), the Lower Leonardian (Wolfcamp A3, A2, and A1), the Dean Formation, and a short section of the Spraberry. Observations were made of the slabbed core, of photos of the core in plain light and ultraviolet light, of thin sections, and of ion milled samples that were examined with a Field Emission Scanning Electron Microscope. Core photos were enhanced using Adobe Photoshop.

The cut face of the core was prepared for examination by sanding it with 100, 200, and 300 grit wet/dry sandpaper and a modest amount of water. The overall fine-grained texture of the rocks necessitated the use of a Bausch and Lomb 7x-30x binocular microscope and multiple light sources to make observations at the hand specimen scale. A small amount of water applied to the surface of the rocks facilitated observation of otherwise obscured textural relationships. A solution of 10% HCl applied to the rocks helped to differentiate siliciclastic from carbonate lithologies. Observations were made on the centimeter scale and recorded in an Excel spreadsheet. The core consists of a thinly bedded mixture of fine-grained siliciclastic and carbonate sediment. Each bed was systematically described using the following criteria:

- Thickness
- Color
- Siliciclastic and carbonate content
- Grain size and sorting
- Grading
- Primary sedimentary features
- Bedding boundaries
- Degree of bioturbation
- Type of trace fossils
- Presence and type of concretions
- Reaction to dilute HCl
- Other distinguishing characteristics.

Assigning numerical values to each category and sub category made it possible to sort the data, to perform statistical calculations, and to integrate the core description with well log, X-ray Diffraction, Rock-Eval, and GRI data. Integration of data from these techniques aids in characterizing the type, amount, and location of minerals and organic matter. A stratigraphic column was generated using Strat-Gen software provided by the Indiana Geologic Survey.

Ninety thin sections prepared by Core Laboratories were examined along with the core. The thin sections were epoxy impregnated and stained for carbonate and dolomite identification. Samples for thin sections were taken in conjunction with samples for X-ray Diffraction at approximately ten-foot intervals for most of the length of the core. An additional fifteen polished thin sections

were made to fill in gaps where sampling by Core Laboratories was inadequate. Thin sections were examined using a Zeiss Photo III petrographic microscope in transmitted light. Microscope images were acquired with a Pixera Pro 600ES digital camera with 5.8 megapixel resolution.

The use of argon ion milled samples and a Scanning Electron Microscope made it possible to characterize porosity, organic matter, and mineral interrelationships at magnifications needed for very fine-grained sediments (Schieber, 2013). Elemental analysis using energy dispersive spectroscopy (EDS) was performed during the SEM study to confirm mineral identification. One or two representative examples of each lithofacies were cut from the core perpendicular to bedding plane. The face of each sample was mechanically polished and then argon ion milled for 2-3 hours. In order to prevent heat damage to the sample face during the ion milling process the ion mill chamber was cooled with liquid nitrogen. The SEM is an FEI Quanta 400 FEG and was made available by the Indiana University Shale Research Lab.

Lithofacies

The stratigraphic intervals present in the core are the Wolfcamp B2, B1, A3, A2, A1, Dean Sandstone, and Lower Spraberry. Lithofacies within each of these intervals were defined based on color, texture, mineralogy, biogenic component, sedimentary structures, and depositional process. Thin section observations and XRD whole rock analysis were used to establish mineralogy. Mudstones were classified using the methods proposed by Lazar, et al., (2010). Carbonate lithotypes are named using Dunham's classification, (1962) and its modification by Embry and Klovan (1971). Facies associations and depositional processes related to each stratigraphic interval will be discussed in the chapter describing depositional processes.

Silty mudstone and Muddy siltstone

The silty mudstone and muddy siltstone lithologies share the same mineralogy and sedimentary structures and are grouped together as a single lithofacies. They only differ in the relative proportions of silt (quartz + feldspar) to clay, and are typically black or dark gray in color. The lower contact may be sharp or gradational. The upper contact may be sharp or gradational when overlain by another clay rich lithology and is erosional when overlain by the packstone-grainstone facies. In many horizons, original upper and lower bedding planes are disrupted by soft sediment deformation.

Silt content ranges from 36-78% and consists mostly of sub-angular to angular detrital quartz grains. Silt size ranges from 20-60 microns. Feldspars are present but make up less than 10% of the silt fraction. Quartz also occurs as diagenetic overgrowths, elongate microcrystalline stringers, replacement of calcareous microfossils, and sponge spicules. Total clay content ranges from 18-39%, and consists predominantly of illite with a lesser amount of mixed layer illite/smectite. There may be up to 3% calcite and or dolomite in the form of scattered, randomly distributed microfossils. Pyrite in the form of evenly distributed poly-framboids is common but not abundant, and contributes 2% to 7% weight to the rock based on XRD. Phosphatic and pyritic concretions are common in the clay rich intervals (Figure 3A).

The silty mudstones and muddy siltstones appear structureless or show crude lamination (Figure 3). Laminae are spaced at the millimeter scale, and show horizontal-parrallel to low angle orientation. Laminae are composed of alternating silt rich and mud rich laminae. In some intervals, (Figure 13 B) the silt laminae appear at the hand sample scale to be sharp and parallel. However, at the thin section scale the laminae are fuzzy and discontinuous. Steeply inclined (> 20°), parallel laminae are present in some places but these are considered to have been originally deposited horizontally and later on reoriented by slumping. Some of the mudstones show a slight lenticular texture at the hand specimen scale. This texture is attributed to a combination of bioturbation, the presence of agglutinated benthic foraminifera, and the accumulation of fecal pellets (Figures 4B and 4C). Differentiating between these three mudstone types is best

accomplished by studying thin sections. Fecal pellets exhibit closer packing and have a smaller size range than do burrows. Burrows tend to be larger and more widely spaced, are silt rich, and give the sediment a distinct mottled texture (Figures 4D and 4F).

Bioturbation is pervasive in this lithofacies and ranges in intensity from moderate to high, resulting in as little as the disruption of individual laminae to the complete homogenization of entire beds. Distinct trace fossils are present in a few beds and were identified as *Chondrites* and *Phycosiphon* (Figure 9D). Both of these trace fossils types are common ichnofabric-forming trace fossils in clay-rich sedimentary rocks (Wetzel and Uchman, 1998). In hand sample, *Chondrites* usually appears as an array of tiny elliptical dots because a vertical oriented cut through the core truncates numerous branching feeding tunnels. *Phycosiphon* burrows are typically composed of dark gray mud cores surrounded by halos of lighter and coarser-grained sediment. *Phycosiphon* is thought to bioturbate up to 15 cm below the sediment-water interface in a wide range of bathymetric conditions from shallow marine to bathyal and perhaps even abyssal depths (Wetzel and Bromley, 1994).

Fecal pellets are common. They are ellipsoidal or fusiform in shape and composed of fine grained quartz silt and clay (Figure 4C). They typically occur in conjunction with agglutinated benthic foraminifera. The alignment of concentrated fecal pellets parallel to bedding plane gives the sediment a weakly laminated or lenticular appearance. Agglutinated benthic foraminifera are common but not abundant and occur as isolated individuals in the mudstone

(Figure 4B). Other biogenic constituents are rare and make up less than 3% of the total sediment volume. They include calcispheres, benthic foraminifera, sponge spicules, and unidentified shell fragments.

Agglutinated benthic foraminifera composed of microcrystalline quartz are flattened and oriented parallel to bedding, may be bent around more rigid particles, and in places have a dark, clay filled, medial suture. These organisms construct their chambers from silt grains that are collected from their surroundings. Silt grains are bound by organic cement (replaced by silica during diagenesis) and there is a clear preference for fine-grained quartz silt (Schieber, 2009).

Silty Calcareous Mudstone

Silty calcareous mudstone typically occurs interbedded with non-calcareous silty mudstone (Figures 3A and 3B). In hand sample, the two are often indistinguishable were it not for their reaction to dilute HCl. The calcareous mudstones are dark gray to medium gray in color. A lighter gray color can be attributed to an increase in carbonate content in the form of carbonate mud, microfossils or silt sized shell fragments. Bed thickness ranges from ½ inch to 1.5 feet. A typical sample has equal amounts of silt, carbonate, and clay and less than 10% pyrite. Silt size ranges from 20-30 microns. Biogenic components include calcispheres, foraminifera, sponge spicules, and other skeletal debris. Partial dissolution and dolomitization of microfossils and shell detritus is

common. Carbonate concretions, ranging in size from ½ inch to 3 inches thick, are present in some intervals (Figure 3E).

Skeletal Argillaceous Wackestone-Packstone

Skeletal argillaceous wackestone-packstones are medium gray to light gray in color and composed of carbonate microfossils and shell debris in a clay and silt rich matrix. Abundant microfossils give skeletal argillaceous wackestone-packstone a distinctive speckled appearance in hand sample, especially when viewed under ultraviolet light (Figure 5A). Individual beds are structureless or weakly laminated. Normal grading, from packstone to silty mudstone is common. Amalgamated beds are also common. Lower contacts are usually sharp. Upper contacts may be gradational or sharp. Individual bed thickness ranges from 1/2 inch to more than 3 feet. Bed thickness is less than 0.5 feet.

Biogenic components consist primarily of calcispheres, benthic foraminifera, and few, fine grained, randomly scattered, shell fragments. Partial dissolution and dolomitization of microfossils and shell detritus is common. Skeletal argillaceous wackestone-packstone is found interbedded with the mudstone and calcareous mudstone facies or as graded successions above the grainstone lithofacies.

Objects identified as calcispheres are spherical or egg-shaped microfossils with walls of calcite and calcite or dolomite cemented interiors. They are commonly interpreted as the remains of calcareous dino-flagellates, or

organisms related to them (Flügel, 2010). Modern calcispheres are only found in areas characterized by shallow, protected waters with restricted or semi-restricted circulation (Marszalek, 1975). However, the biological affinity of most Paleozoic calcispheres remains uncertain making them of limited value for paleoenvironment reconstructions (Berkyova, 2010).

Foraminifera are small, predominantly marine heterotrophic protists that construct chambered shells (Flügel, 2010). Most foraminifera seen in this core and thin sections are less than 1 mm in size. Because planktonic foraminifera do not appear in the rock record until the Early to Middle Jurassic (Tappan and Loeblich, 1988), the observed foraminifera are interpreted to be benthic organisms, derived from the surrounding platform and slope environments and delivered into a deeper water setting by bottom currents or low density muddy turbidites.

Skeletal Grainstone

Skeletal grainstones are composed of medium to fine grained carbonate debris, carbonate lithoclasts, and silty mudstone clasts (Figure 6). Individual beds are normally graded and may exhibit a range of sedimentary structures including cross lamination, parallel to wavy lamination, and contorted bedding. Contact with underlying sediments is sharp and erosional with well-defined scour features. The upper contact is typically gradational. Bed thickness ranges from 1/2 inch to over 2 feet. The average bed thickness is 3 inches. The

assemblages of skeletal debris and carbonate lithoclasts found in this facies appear derived from shelf margin depositional environments. Fossil material consists of shell fragments, phylloid algae, foraminifera, *Tubiphytes*, and sponge spicules. The grainstone facies is pervasively cemented by either calcite or dolomite. Partial dissolution, as well as partial to complete dolomitization of carbonate grains is common. Sand-to-pebble sized, flattened and deformed mud clasts that share the same composition as the underlying mudstones are common. Nodules and concretions eroded from underlying mudstone beds are found at the base of the grainstone beds as shown in Figure 3F.

Bioclast-Lithoclast Wackestone-Floatstone

This facies is composed of diverse carbonate particles greater than 2mm in size that float in a dark gray, silty, argillaceous or carbonate mud rich matrix (Figure 7A). Sedimentary structures are mostly absent though some beds exhibit weak lamination. Cobble sized, flattened and internally deformed, mud clasts are common, occurring within the bed or close to the upper surface of the bed (Figure 7B). Angular limestone blocks of shelf margin origin are present in some beds (Figure 3C, 7C). Lithoclasts that are similar in composition to the matrix are present but difficult to differentiate. Bed thickness ranges from 4 inches to 8.5 feet.

Ash Beds

Ash beds occur infrequently. They are easily recognized by their bright orange color under ultraviolet light or gray-green color in hand sample. They are composed of sand sized volcanic clasts and scattered mineral grains in a matrix of clay, mica, quartz, and feldspars. Some of the beds are normally graded and banded while others display no sedimentary structures. Bed thickness ranges from 0.5 to 6 inches.

Silty Sandstone

This facies is composed of well sorted, very fine sand and silt sized grains of quartz (35-65%) and feldspar (10-15%) with a minor amount of clay (10-13%).(Figure 12) The sandstones are tan to light gray in color. Individual beds range in thickness from 3 inches to 9 feet. Lower contacts are usually sharp and irregular and sometimes display load casts. Upper contacts are gradational with the laminated and bioturbated siltstone facies. The thick bedded sandstone beds typically have a massive lower section with distinctive fluidization structures caused by upwards escape of pore water. Sedimentary structures include parallel laminations, low angle cross-laminations, contorted bedding, flame structures and other soft sediment deformation structures. Bioturbation is absent except in the upper division of some of the thicker sandstone beds. All of the sandstone beds are well cemented by calcite, dolomite, or quartz.

Laminated to Bioturbated Muddy Siltstone

Laminated and bioturbated muddy siltstones occur interbedded with massive, silty sandstone and silty mudstone. Silt size ranges from 30-60 microns. Upper and lower bed boundaries are sharp in the beds that retain well-defined lamination. Most beds display fine, parallel, discontinuous, wavy to horizontal laminations that are disrupted by cryptobioturbation (Figure 8). In hand sample the laminations look relatively sharp and continuous (Figure 13B), however, when viewed in thin section the laminations lack definition, are wavy, and discontinuous (Figure 8C).

Bioturbated siltstone beds occur in two contexts; as beds that are gradational with underlying sandstone and overlying silty mudstone or interbedded with laminated siltstone and silty mudstone. Highly bioturbated beds have no remnant laminations and sometimes exhibit well developed ichnofossils that include *Chondrites*, *Thalassinoides*, and *Phycosiphon*. The degree of bioturbation ranges from moderate, wherein discreet traces are easily identified, to mottled wherein the sediment is thoroughly mixed with some traces remaining identifiable, to beds that are completely homogenized.

Mineral composition includes quartz, clay, feldspars, and trace amounts of pyrite. Quartz content ranges from 44-59%, clay content from 18-32% and feldspars from 11-15%. This facies is pervasively cemented by calcite, dolomite, quartz, or ankerite. Bed thickness ranges from 3 inches to 4 feet.

Depositional Processes

Slides and Slumps

Sliding and slumping are two types of gravity driven submarine sediment mass transport processes that are capable of moving huge amounts of sediment from a shallow to a deep water setting. The process of sliding or slumping may cause the breakup of beds and with continued flow, it is possible for a slide or slump to start a whole range of other gravity driven transport processes including debris flows, turbidity currents, and grain flows (Reading, 1996, Hüneke and Mulder, 2011; Talling et al., 2012). Although slides and slumps may be part of a continuum of gravity driven processes, each has distinct depositional features related to the degree of internal deformation of the sediment mass. Slides and slumps require a slope to become active and may be initiated by sediment overloading, excessive pore water pressure, and seismic activity.

Submarine sliding involves the movement of an internally undisturbed mass along a discreet shear surface. Slides involve large blocks of lithified or partially lithified sediment that move in isolation or as clusters in continuous contact with the underlying sediments. The bulk of the displacement is concentrated on a basal slip surface. Blocks of sediment lack internal deformation features, however, with downslope movement slide masses may show progressive fragmentation and grade into a slump (Lewis, 1971).

A slump originates from mass sliding and creeping of semi-consolidated sediment that can occur in deep or shallow water environment (Flügel, 1990).

The bulk of moving material is commonly unconsolidated and undergoes complex internal deformation caused by extensional, compressional, and shearing forces as it moves down slope (Reading, 1996). It may be possible to recognize remnants of original bedding and lamination, depending on the extent of deformation. Key features of slump deposits include the convolution and distortion of beds, the presence of undeformed beds above and below, erosional truncation of folds at the top surface, and the restoration of horizontal bedding immediately above the top surface.

In the Wolfcamp B2 and B1 intervals there are thick sections of muddy, sediments that appear to have undergone slumping prior to significant consolidation. Slump features include sheared and rotated semi-consolidated beds (Figure 3H), pinch and pull-apart structures (Figure 7E), and chaotic intermixing between unconsolidated clay rich beds (Figures 9B, 9C).

Debris Flow Deposits

Subaqueous debris flow has long been recognized as a major sedimentary process on continental and basin slopes (Asku, 1984). The term *debris flow* refers to the sluggish downslope movement of cohesive mixtures of granular solids, clay minerals, and water in response to the pull of gravity (Middleton and Hampton, 1973). Cohesive flows are differentiated from all the other flows because they have enough cohesive material to impart a pseudo-plastic rheology resulting in a reduction of the rate at which they can dilute by

either particle deposition or entrainment of ambient water. Thus they tend to hold together (Mulder and Alexander, 2001). Debris flows may be initiated by failure of overloaded slope sediments in the form of a large catastrophic event or the accumulation of many small failures. In debris flows, solids are supported by and transported by a cohesive matrix of clay and water. The presence of clay gives the mixture its coherent nature and is important for sustained movement. Buoyant support of the grains and clasts by a cohesive matrix rather than turbulence, upward escape of fluid, or grain dispersive pressure distinguishes true debris flows from turbulent flows, fluidized flows, and grain flows. Because most of the bed shear is concentrated near the base of the flow, a debris flow experiences greater grain dispersive pressure at the bottom of the sediment column than at the top (Bagnold, 1954; Lowe, 1982; Mulder, 2011; Talling et al., 2012). This difference results in a net upwards directed force that tends to push large clasts upwards. A debris flow moves as long as the gravity imposed shear stress exceeds the yield strength of the flow, and once the shear stress falls below that value the flow freezes *en masse.* In *en masse* settling, deposit thickness is closely related to flow thickness (Middleton and Hampton, 1973; Iverson, 1997; Talling, et al., 2012).

The most common feature of a debris flow deposit is a poorly sorted, massive bed of sediment having a multimodal size distribution. Other criteria for recognizing debris flow deposits include i) a lack of vertical grading except for outsized clasts; ii) lack of sedimentary structures formed by bedload reworking; iii) a sharp grain-size break at the upper boundary of the debris flow; and iv) mud

clasts that, if present, are chaotically distributed (Talling, et al., 2012). Thinner deposits may show faint lamination, reverse grading, water escape structures, and outsized clasts. Bedding plane features include load casts and tool marks. Although debris-flow deposits are characteristically very poorly sorted and may show few if any internal structures because of plug flow and *en masse* deposition, remnants of shear fabric may be visible near the flow base and margins and also within the flow because of flow surging (Mulder and Alexander, 2001). In addition, material at the sides or front of the flow can come to a halt first with the center of the flow remaining fluid for longer (Talling, et al., 2012).

The silty argillaceous bioclast-lithoclast wackestone-floatstone facies is interpreted as a debris flow deposit (Figure 7A). This interpretation is based on the presence of a silt and clay rich matrix with scattered lithoclasts and bioclasts. Less common are beds that are clast supported, having less than 25% matrix. None of the debris flow deposits show grading, internal bedding, lamination, or sorting of clasts although lofting of flattened and internally deformed, cobble sized mud clasts to the top of beds is seen in some places (Figure 7B). Seen at the upper boundary of the debris flows is a sharp transition from the debris flow deposit to mudstone.

Turbidity Current Deposits

Turbidity currents support sediment by fluid turbulence that prevents the setting of entrained particles. The downslope movement of a turbidity current is

due to the density contrast with the surrounding water (Bouma, A.H., 1962, Bouma and Stone, 2000; Lowe, D.R., 1982; Middleton and Hampton, 1973; Talling et al., 2012)). The deceleration of a turbidity current deposits beds with a range of characteristic internal structures that vary vertically and laterally along the transport path. Key indicators of turbidity current deposition include the following (Bouma, A.H., 1962, Bouma and Stone, 2000; Lowe, D.R., 1982; Middleton and Hampton, 1973; Mutti & Ricci Lucci, 1975; Stowe and Mayall, 2000):

- Graded bedding and current ripple laminations that alternate with beds deposited by suspension settling.
- Suspension fall-out dominated intervals that show an intensification of bioturbation towards the top, including distinct burrows and disruption of lamination. (Stowe and Shanmugam, 1980; Mulder, 2011).
- Scour marks at the base of the turbidite bed caused by the erosive action of turbidity currents.
- Regular vertical sequence of units characterized by specific sedimentary structures (Bouma, A.H., 1962)
- Uniform current direction.
- The presence of different fauna in the turbidite and adjacent pelagic or hemipelagic beds.

There are three varieties of turbidity current deposit identifiable within the core: low-density, low-energy mud rich turbidites, medium to high-density

carbonate turbidites, and high-density, fine grain, siliciclastic turbidites. Each type has unique sedimentary structures that reflect the density of the flow, energy and duration of flow, the location of deposition along the flow path, and the grain type and size.

The Wolfcamp B2 section contains numerous low-density and low-energy turbidity current deposits that constitute the skeletal argillaceous wackestone-packstone facies (Figure 5). The presence of abundant calcispheres and foraminifera in a clay and silt rich matrix makes this type of turbidite unique. The transportability of the microfossils in a low density turbidity flow is a function of variations in grain shape and density, not grain size alone. A solid grain equivalent in size to the foraminifera and calcispheres would be too heavy to be transported by low-density turbidity flow, assuming that the microfossils were remobilized before infilling of the hollow shells occurred. These beds are thin, sometimes normally graded, sometimes weakly laminated, but are most often structureless (Figures 5A, 5B). They have a sharp base typically underlain by mudstone or wackestone. At the base of some of these deposits, there is a 1-2 mm, light gray, calcite-cemented layer. The upper bed boundary may be sharp or gradational with calcareous mudstone beds. These beds are interpreted as deposits of episodic, waning, low density, low energy turbulent flows. Low density, mud-rich turbidites are difficult to distinguish from other fine grained sediments deposited by suspension settling or bottom currents as they may be homogenized by bioturbation.

The Wolfcampian B1, A3, A2, and A1 intervals are dominated by medium to high-density turbidites that are composed of carbonate debris sourced from the shelf margin. These turbidites beds are typically less than 6 inches thick and display internal structures consistent with Bouma divisions Ta through Te (Bouma, A.H., 1962), though complete sequences are uncommon (Figures 10, 11A).

The Dean interval is dominated by fine grained siliciclastic turbidites with little textural or compositional variation (Figure 12). The most distinctive feature of these turbidites is the thick, massive lower section that displays abundant fluid escape channels. Other distinctive features include a scoured base, load casts, flame structures, an upward increase in clay content, and an intensely bioturbated upper division.

Suspension Settling and Bottom Current Deposits

Density flow deposits are often separated by hemipelagic mud layers formed by settling of sediment particles from the ocean in the time period between density flows (Talling et al., 2012). Hemipelagites are fine-grained sediments deposited in a marine environment with both a biogenic and terrigenous component. The primary way in which hemipelagic sediment is differentiated from pelagic sediment is by provenance. Hemipelagic sediments are composed of a mixture of at least 25% silt and clay derived from a terrestrial source plus carbonate mud and widely dispersed calcareous microfossils derived

from shelf and slope environments (Einsele, 1992; Nichols, 2009; Henrich and Hüneke, 2011). The fine grained terrigenous component of hemipelagites may originate from multiple sources: windblown dust from arid and semi-arid areas, fluvial sediment carried onto the shelf as freshwater plumes off river mouths, fine volcanic dust, or from fine-grained sediment stirred up on the shelf by storms and redistributed offshore by currents (Reading, 1996). Once in suspension and in the absence of bottom currents, the sediment settles through the water column and is deposited on the shelf or slope. Alternatively it may have sufficient excess density to sink as very dilute, slow moving density flows which move downslope under the influence of gravity (Reading, 1996).

Hemipelagic sediments are seen throughout the core but are most commonly associated with the upper unit of turbidite beds where a fine-grained mixture of pelagic and terrigenous detrital sediment is deposited by slow fallout from suspension. The origin and hence the general composition of the hemipelagic deposit is the same as that of the turbidite. As seen in Core X the hemipelagite beds are relatively homogeneous, crude or no lamination, may show normal grading, have a sharp or gradational base that is not erosive, and may be bioturbated (Figures 11D and 13C). The silty mudstone, muddy siltstone, and calcareous mudstone facies deposited by suspension settling display a range of bioturbation intensity such that any original sedimentary fabric and associated sedimentary structures are disrupted or entirely destroyed. This results in the mixing of sediments within and between beds though some remnant of the original depositional fabric may remain. Also, much of the fine-

grained sediment of hemipelagic origin shows evidence of having undergone slumping and sliding which served to further obscure primary depositional structures. In the absence of any primary depositional structures it is difficult to differentiate between hemipelagic sediments deposited by suspension settling and those deposited by bottom currents or slow moving, low density turbidity currents.

Hemipelagic material may also be resuspended, transported, and deposited by bottom currents. Bottom currents are thermohaline induced, generally slow moving (10 cm/sec) currents active in deep-water setting. In general, most terrigenous detrital sediment is deposited at or near the seafloor where rivers meet the coastal ocean (Henrich and Hüneke, 2011). Mud is transported via turbid plumes and hyperpycnal flows, spreading across the shelf under the combined influence of buoyancy, gravity, shelf currents, and Coriolis forces (Mulder, 2011; Henrich and Hüneke, 2011). While much of the mud ends up on the shelf a certain amount is transported to the shelf margin and slope. The material crossing the shelf break is generally transported either in suspension as a nepheloid layer or as gravity driven density flows (hyperpycnal flows) (Salon et al. 2008; Henrich and Hüneke, 2011). Another possibility for sediment to bypass the shelf is by long-distance transport in the form of sediment-laden highly buoyant surface plumes (hypopycnal flows) (Mulder, 2011; Henrich and Hüneke, 2011). Diffusive transport by waves and tides and advective transport by bottom currents are assumed to control the mud

distribution on the margins and gravity-driven flows are thought to be important for moving sediment down the slope (McCave, 1972; Mulder, 2011; Henrich and Hüneke, 2011).

Some intervals of silty mudstone, muddy siltstone, and calcareous mudstone facies show evidence of having been deposited by bottom currents or slow moving low density turbidity flows rather than suspension settling. This evidence includes normal and reverse grading of beds, a sharp and erosive lower contact, continuous and discontinuous parallel lamination, and thin, discontinuous silt stringers (Figures 8A and 9E).

Depositional Environment

This section provides an interpretation of the depositional conditions that existed during the formation of each major stratigraphic unit. This interpretation is based on the spectrum of primary physical sedimentary structures and their presence in certain combinations as well as major changes in mineralogy, grain texture, and bioturbation. Figure15 illustrates the various envisioned depositional environments in the Midland Basin during early Permian time. Marked on the diagram is the inferred location of the core within the basin during the time of deposition.

Wolfcamp B2-B1

The Wolfcamp B2-B1 interval is composed of seven complexly interbedded lithofacies deposited in a deep water, base of the slope environment:

1. Silty mudstone
2. Muddy siltstone
3. Silty calcareous mudstone
4. Skeletal argillaceous wackestone-packstone
5. Skeletal packstone-grainstone
6. Bioclast-lithoclast wackestone-floatstone.
7. Ash beds

Deposition occurred during a time of widespread platform submergence interrupted by periods of slight emergence and shoaling of the platform. Platform

facies consisting of shallow shelf carbonates and deeper shelf interior sediments transition basinward into mostly mudstone and detrital carbonates facies deposited during times of relative sea level highstand (Mazzullo and Reid, 1989).

Mudstone and siltstone lithologies are composed primarily of fine-grained terrigenous material, organic matter, carbonate mud, and carbonate microfossils. Microfossils include calcispheres, foraminifera, and agglutinated benthic foraminifera that are widely and randomly dispersed throughout the matrix. Beds interpreted as hemipelagites deposited by suspension settling are relatively homogeneous, show poorly developed or no lamination, show little or no grading, and have a sharp or gradational base that is not erosive. Thin ash beds, also deposited by suspension settling, are relatively undiluted by hemipelagic sediments. Beds that show normal and reverse grading of, a sharp and erosive lower contact, continuous and discontinuous parallel lamination, and thin, discontinuous silt stringers are interpreted as having been deposited by bottom currents or dilute, slow moving density flows. A lack of primary sedimentary structures is common and attributed to mixing of the sediment by bioturbation and by post depositional gravity-driven flow processes.

The skeletal argillaceous wackestone-packstone and skeletal packstone-grainstone facies were probably deposited by low to medium density turbidity currents initiated by point or line slope failures. The turbidite currents traveled as sheet or shallow channelized flows and were deposited at the toe of the slope as amalgamated sheets and wedges seaward of the platform margin.

Large portions of the beds are internally convoluted and distorted indicating that they have been remobilized by gravity-driven flow processes prior to significant consolidation or cementation. Remobilization had the effect of altering or destroying many primary sedimentary features. The most common gravity flow deposits seen in the B2-B1 intervals are slumps and debris flows. Thick debris flow deposits are likely a result of major, episodic events in which large sections of the platform margin collapsed and correspond to periods of relative sea level lowstand (Mazzullo and Reid, 1989; Hamlin and Baumgardner, 2012).

Wolfcamp A3-A2-A1

The transition from the Wolfcamp B2-B1 to the Wolfcamp A3-A2-A1 marks an abrupt change in depositional character from combined hemipelagic settling, debris flows, and slumps to turbidity current deposition of carbonate debris shed from the shelf margin. This region-wide change is attributed to an increase in the rate of basin subsidence and rapid sea level rise that cut off the supply of siliciclastics into the basin. Consequently, the Northern and Eastern shelves transformed from a ramp and distally steepened ramp system to a rimmed margin shelf system (Mazzullo and Reid, 1989). In addition, climate in the region changed from humid to arid. The transformation in shelf morphology resulted in the deposition of thick, cemented, wave resistant, carbonate bank and reef build-ups along the shelf margin. The rapid vertical accretion of the shelf margin led to

the constant shedding of carbonate debris onto the shelf margin slope where the debris was subsequently transported into the basin by turbidity currents initiated by slope failure. This scenario fits the sea level "highstand shedding" model proposed by Schlager et al. (1994) in which maximum delivery of carbonate debris to the basin is concurrent with maximum carbonate production during sea level highstand.

The Wolfcamp A3 and A2 intervals are characterized by the deposition of fine grained carbonate turbidites. These turbidites can be identified through a vertical succession of sedimentary structures, such as complete and incomplete Bouma sequences (Figure 14), bedding characteristics, and changing lithology. Mazzullo and Reid (1989) attribute the abundance of detrital carbonates in the lower Leonard to (1) the great thickness of shelf margin reefs, (2) considerable shelf to basin relief, (3) steep fore-reef slopes that provided a constant supply of carbonate debris to the basin, and (4) increased accommodation due to rapid basin subsidence.

Moving upwards through the Wolfcamp A3 and A2 interval, carbonate turbidite beds become thinner and occur less frequently. Silty mudstone and muddy siltstone beds become thicker and occur more frequently. This change reflects either a decrease in carbonate production on the shelf or a change in the relative location of carbonate production on the shelf. Intervals dominated by carbonate turbidites formed during periods of maximum carbonate production and/or platform progradation. Intervals that are dominated by terrigenous clastics sediments represent periods of sea level lowstand when terrigenous clastics

migrated basinward, were transported across the shelf, and delivered to the basin by way of feeder channels. Sea level lowstands are associated with high terrigenous load, widespread erosional discontinuities on the shelf and slope, and active development of large turbiditic systems on the continental rise (Talling et al., 2012).

An increase in the proportion of terrigenous clastic sediment relative to biogenic sediment might also be related to drowning of the carbonate platform. A reef or platform is drowned when relative sea level rise outpaces platform growth such that the platform top becomes submerged below the photic zone and no longer produces sediment. When carbonate production diminishes, highstand shedding ceases and the entire system reverts to pelagic or hemipelagic sedimentation (Schlager et al., 1994). Based on the identification of multiple shoaling upward cycles in shelf strata that are coeval with the Wolfcamp A3, A2, and A1 intervals and evidence of subaerial exposure at the tops of shelf patch reefs (Hobson et al., 1985; Mazzullo and Reid, 1989; Montgomery, 1996), the most likely scenario for the siliciclastic-dominated intervals is one in which sealevel lowstand led to sediment bypass of the shelf.

The A1 interval shows a near cessation of fine grained carbonate turbidites and an increase in silt and fine sand content that corresponds to the emergence of the platform. Siltstone and fine sandstone beds gradually become more common and increase in thickness upwards. The style of bioturbation also changes with burrows increasing in intensity and diversity.

Dean Formation

The transition to the Dean Sandstone marks a significant basin-wide change in sediment type and source, from a carbonate dominated system to a siliciclastic dominated system. The interval below the Dean is characterized by carbonate turbidites that gradually diminish in thickness and frequency upwards in response to shorter periods of sea level highstand. Up section they are gradually replaced by silty calcareous mudstones and muddy siltstones. The Dean, by contrast, is composed of thick, tan and gray colored, very fine grained sandstone beds that grade upwards into laminated siltstone and silty, bioturbated, mudstone. The sandstone beds have a massive lower section with fluidization structures, parallel laminations, low angle cross-laminations, contorted bedding, flame structures and other soft sediment deformation structures. Bioturbation is absent in the sandstone beds (Figure 12).

The laminated siltstone and silty, bioturbated mudstone beds that overlie the sandstone beds display fine, parallel to wavy, discontinuous, horizontal laminations that are disrupted by cryptobioturbation (Figure 8). The deposition of these laminated siltstone beds is attributed to traction deposition and suspension settling from waning turbidity currents. In some intervals the laminated siltstone beds occur interbedded with mudstone beds (Figure 13B) rather than gradationally with underlying sandstone beds. These laminated siltstones may represent either the distal levee deposits of turbidite flows or reworking and bedload transport of previously deposited sediments by bottom currents. Distinguishing between deposits of the two processes is problematic because

both create similar bedforms and the interplay of the two is the rule rather than the exception for deep-water sedimentation (Faugeres and Stowe, 1993). Hamlin, 2010, attributes the deposition of the Dean interbedded mudstone and laminated siltstones units to background sedimentation away from active sediment gravity flows. Sediment gravity flows responsible for these deposits may have been initiated by ebb flow following storms or by slumping along the shelf margin and slope.

The shelf equivalent of the Dean is the Tubb Formation which includes sandstones, anhydritic shale, bedded evaporites, and shallow marine dolomites (Hobson et al., 1985; Mazzullo and Reid, 1989). Shelf deposition occurred in a complex of eolian, desert fluvial, peritidal, and nearshore environments during a time of gradual relative sea-level fall which culminated in complete shelf emergence (Silver and Todd, 1969). Recorded in the shelf deposits are multiple small-scale cycles of sea level change, superimposed on an overall sea level fall during this period (Mazzullo and Reid, 1989). Two distinct units, consisting of stacked turbidites that show an increase in sandstone bed thickness upward through each unit, are observed in the Dean portion of the core. Both units are approximately 80 feet thick. Beds range in thickness from 3 inches to 9 feet. These sandstone beds show very little variation in grain size and are separated by intervals of laminated or bioturbated siltstone and mudstone. The upper part of the Dean, following the second unit of sandstone turbidites, is composed primarily of interbedded siltstone and mudstone.

Deposition of the Dean Formation was primarily by turbidity currents and associated suspension settling. Evidence of turbidity current deposition can be seen in the well-developed bedforms and sedimentary structures that correspond to Bouma divisions Ta through Te (Figure12) and in the fine sediment grade that can be supported by the upward component of fluid turbulence. Each turbidite deposit shows a transition from sedimentation dominated by traction to sedimentation dominated by suspension fallout. The suspension fall-out dominated intervals show an intensification of bioturbation towards the top, including distinct burrows and disruption of lamination.

Origin of Sand and Silt

The Late Paleozoic origin of silt and sand in Delaware and Midland Basin deep water deposits has been the subject of numerous of papers (Fischer and Sarnthein, 1988; Kocurek and Kirkland, 1998; Hamlin and Baumgartner, 2012; Soreghan and Soreghan, 2013). It appears that although the original source of the silt and sand may be the same for deposits ranging in age from Wolfcampian to Guadalupian, the entry points of the sediment into the basins varied with time and changing wind patterns.

In earlier investigations (Kocurek and Kirkland, 1998; Fischer and Sarnthein, 1988) sedimentological data, stratigraphic correlations, paleogeography, paleowind data, and facies distributions were used in combination to propose that during Leonardian time the silt and sand were derived from contemporaneous aeolian systems to the northeast of the basin.

Isopach and net-sandstone maps published by Hamlin and Baumgartner (2012) confirm the northeastern origin of the sediments. The maps show persistent thinning of the Spraberry intervals from north to south indicating that sediment was dispersed across the Northern Shelf margin and transported longitudinally down the axis of Midland Basin. They also found that the older, Wolfcampian aged thickness patterns suggest a siliciclastic sediment source more to the south and east.

Soreghan and Soreghan (2013) used detrital zircon geochronology to define potential bedrock source regions and to trace clastic delivery to the Permian Basin. They found that the combined mineralogy and provenance spectra of the younger, Guadalupian aged, clastic sediments deposited in the Delaware Mountain Group pointed to sources in the Ouachita system, including possible recycled Appalachian detritus. Key sources of sediment may have been within terranes accreted and uplifted south of the Ouachita suture, now located in Mexico and Central America (Soreghan and Soreghan, 2013). Dispersal pathways likely involved a component of fluvial transport draining the source areas and the eventual wind driven deflation of these fluvial deposited sediments. Winds blowing from the east-southeast and subordinate seasonal winds from the west-northwest moved silt and sand into the Permian Basin region. During low sea level and shelf emergence, sand and coarse silt, in the form of dunes, migrated to the shelf edge where slumping of the seaward face of the dunes generated density flows that transported sand into the basin (Fischer and Sarnthein, 1988).

The production, transportation, and deposition of silt and clay are ultimately controlled by climate (Tsoar and Pye, 1987). During periods of humid climatic conditions, fluvial transport of silt dominates. The presence of moisture and abundant vegetation retards wind entrainment of fine grained sediments. During periods of arid climatic conditions wind transport of fine sediment dominates. Dry source areas with little vegetation allow for sand saltation and ballistic entrainment of silt particles, a process that enhances silt deflation and transport by wind.

Coarse silt and sand seen in the core share some characteristics of aeolian transport. They are composed of quartz and feldspar, are well sorted, fine grained, contain very little clay, and show little to no textural grading. Other common characteristics of aeolian transport such as grain frosting and iron staining are noticeably absent. The presence of silt in all lithofacies throughout the core indicates that silt was supplied constantly but at variable rates to the basin. It is likely that both fluvial and aeolian processes account for delivery of silt and clay to the basin. Studies of aeolian transport mechanisms have shown that the size of wind blown silt ranges from up to 50 microns close to the source region to about 0.1-20 microns in far distal areas after long distance transport in the atmosphere (Bagnold, R.A., 1941; Tsoar and Pye, 1987; Talling et al., 2012). Medium and coarse silt fractions are transported mainly in short-term suspension or saltation, deposited near shore and subsequently transported across the shelf by bottom currents and turbidity flows to the basin. Silt particles finer than 20

microns are transported in long-term, air-borne suspension and are widely dispersed.

Deep water sand beds found throughout the Midland Basin of the same age share many similarities (Hobson et al., 1985; Mazzullo and Reid, 1989; Silver and Todd, 1969) ; they are composed of well sorted, fine grained, quartz and feldspars, contain very little clay, show little to no textural grading, and commonly display the characteristics of deposition by turbidity current. The sand beds typically grade into stuctureless, bioturbated silty mudstone.

The finely laminated silty mudstone beds composed of silt and clay were likely deposited by bottom currents. Bioturbation of laminated siltstone beds is ubiquitous and ranges from moderate to high. The degree of bioturbation is related to a variable rate of deposition. During periods of slow sedimentation, organisms had more time to disturb the sediment leading to beds that retain little of the original depositional fabric. During periods of rapid sedimentation, organisms had less time to disturb the sediment allowing the sediment to retain its original depositional fabric.

Scanning Electron Microscope Investigation

Petrographic examination of porosity in shale and other low permeability rocks requires electron microscopy (Schieber, 2013). The purpose of this SEM investigation is to identify the morphology and distribution of pore types and organic matter found in each facies. Pores and associated pore networks are a function of original matrix mineralogy, fabric (arrangement of grains), texture (size and sorting of grains), organic matter composition, and the combined effects of deposition, compaction, cementation, dissolution, and thermal maturation (Loucks et al., 2012). Pore type and distribution defines the permeability of the rock, controls the storage and flow capacity (migration) of hydrocarbons, and can influence mechanical properties relevant to well bore stability and hydraulic fracturing (Slatt and O'Brien, 2011). The pore types that are likely to natural or enhanced permeability are those that are interconnected.

Observations were made on argon ion milled samples with a field emission scanning electron microscope. This approach enabled the visualization of various micron and sub-micron pore types in bedding-perpendicular surfaces for each lithofacies. Special care was taken when preparing samples to eliminate mechanically induced surface artifacts that might be mistaken as pores (grain plucking) and to minimize heat induced shrinkage cracks during the ion-milling process.

As mentioned above, three principal types of pores were identified in the various lithofacies: framework pores, organic matter pores, and dissolution pores.

All pore types occur to some extent in each lithofacies, however, the dominant pore types in the clay rich facies are framework and organic matter pores. Porosity in the heavily cemented carbonate and sandstone facies is attributed primarily to dissolution.

Phyllosilicate Framework Pores

Framework pores occur wherever the component grains are arranged in such a way as to create a pore space between the grains. The term interparticle porosity is typically used to describe pores of this type but the term does not capture the various pore geometries that result from mineralogy, primary pore preservation, and diagenesis. A phyllosilicate framework pore is formed by the random, edge-to-face packing of clay grains and is analogous to intergranular pores found in coarser grained rocks (Figure 15A, 15B). Framework pores are most often preserved in the pressure shadows of larger, more rigid grains that resist compaction, in the spaces between rigid grains, and where clay grains are bent or splintered during compaction (Schieber, 2013). In the samples taken from the core, both detrital and diagenetic grains create locations for framework pores to be preserved. The pores in these samples range in size from 50 nanometers to 0.5 micrometers.

Phyllosilicate framework pores have been described in several other shale formations. Slatt and O'Brian (2011) proposed that the edge-to-face particle arrangement of clay flakes seen in the Barnett and Woodford shale formations is a result of the preservation of the original depositional fabric within clay floccules.

However, they offer no explanation as to how the open framework could have survived burial and diagenesis. It is likely that during dewatering and compaction, the flocculated clay fabric collapses and the best chance for preservation of phyllosilicate framework pores is in areas where compaction is minimized, such as in the pressure shadows of rigid detrital grains, within fossil interiors, or where diagenetic grains serve as a proppant (Schieber, 2013).

Organic Matter (OM) Pores

In organic rich rocks the pore volume contained within organic matter can constitute a substantial fraction of the total porosity. Observations of core samples from this study indicate that in the clay rich facies OM pores make a significant contribution to the overall porosity. It is common for marine sedimentary rocks to contain a mixture of organic matter types, and those identified in these samples are structured OM and amorphous OM. Amorphous OM is commonly described as amorphinite or bituminite by organic petrographers and is considered to represent bacterially degraded marine organic matter (Schieber, 2013). It is commonly associated with oil prone Type I and II kerogen (Tissot and Welte, 1984). The structured OM has two possible sources: Type II kerogen, such as *Tasmanites* algal cysts and praesophyta (brown algae/kelp) debris or Type III kerogen, produced from the lignin of the higher woody plants that grow on land. In this study, no conclusions are drawn as to the origin of the structured organic matter.

Of the two types of organic matter observed in the core, amorphous OM is the most commonly observed. It consists of Type I and Type II kerogen as determined by Rock-Eval pyrolysis. Organic matter pores visible with SEM appear to occur exclusively within amorphous organic matter. These pores, created during the generation of hydrocarbons, are in the sub-micron range and are round to oblate in cross-section (Figure 16A). OM particles in these samples are typically in the range of 2 to 6 micrometers. OM occurs throughout the matrix as dark irregular patches and wispy specks between mineral grains and within triangular framework pores. The OM patches in these samples sometimes have a sponge like texture (Figure 18A). It is not possible from two-dimensional images to determine if the organic matter displays connectivity in three dimensions, however, it has been reported by Loucks et al., 2012 that OM pores do form an effective pore network.

Structured organic matter is seen primarily in the fine grained carbonate and siliciclastic turbidite facies. Structured OM is black under backscatter imaging, has a smooth texture, and has well defined edges. Individual pieces of structured OM found in these samples are generally larger than pieces of amorphous organic matter and display few if any visible pores.

Abundant organic matter pores should only be expected in rocks that have reached thermal maturity greater than 0.6% R_o (Schieber, 2013). This is consistent with observations of the Marcellus Shale and New Albany Shale made by Schieber, 2013, and the Barnett Shale by Loucks et al., 2011, and Milliken et al., 2013. PI and Tmax values determined from Rock Eval data for this core

range from 0.15 to 0.3 and 430° to 470° C, respectively. The calculated thermal maturity of the rocks is 0.7% to 1.0% R_o, well within the oil window.

Dissolution Pores

Dissolution pores observed in samples from the core form open spaces along the margins or within biogenic carbonate grains, dolomite cement crystals and calcite cement crystals. Dissolution along grain margins creates a thin, uneven, curved volume between the grain and the surrounding matrix. This pore type is most common in the pervasively cemented, low porosity, low permeability, grainstone facies and does not appear to contribute significantly to the overall porosity of the rock. Both resedimented grains and diagenetic cement crystals exhibit dissolution pores indicating that the pores are secondary porosity features that developed after cementation took place. Secondary porosity development through corrosion of carbonate grains implies acidic pore waters and a drop of pH (Schieber, 2013), possibly related to the generation of organic acids, CO_2, and H_2S associated with increasing thermal maturity during burial of these sediments (Mazzullo, 1997).

Fluid generated relatively early on by shale dewatering, during either compaction or mineral transformation, does not have the acidity to generate significant dissolution. Such fluids instead appear to cause more porosity reduction by cementation than porosity increase by dissolution in either the sandstones or carbonates through which they migrate (Mazzullo, 2004). In clay

rich rocks, early diagenetic fluids may serve to preserve porosity by causing the precipitation of diagenetic grains that prop open phyllosilicate framework pores (Figure 17A).

Routine Core Analysis Data

Porosity and Permeability

Porosity and permeability measurements are used to define storage capacity and the conductivity of the rock for fluid flow. Porosity is the volume of the non-solid portion of a rock filled with fluids, divided by the total volume of the rock and is a function of rock type and arrangement of grains. Pore area and pore connectivity control permeability.

The data presented here relate the porosity and permeability measurements obtained by routine core analysis to lithofacies. "Routine" or "conventional" core analysis is a method of study used to determine the basic petrophysical properties of cored rock samples. This procedure employs a small sample to represent an interval of core and produces acceptable results when the pore system is relatively homogeneous. Conventional core analysis plugs are usually collected once per foot or three to four times per meter (Monicard, 1980). Sampling can be done statistically at the mid-point of each foot or the most representative sample in each foot can be selected. Heterogeneous or thinly bedded formations may require a more targeted approach to sample collection in order to achieve a representative sample of each lithology.

Core Laboratories performed the collection and analysis of 716 samples from the core. Samples were collected at approximately ½ foot to 2-foot intervals. Tables 4, 5, 6, and 7 show the average porosity and average permeability for each facies, arranged by stratigraphic interval. Across all

intervals, silty, clay rich facies have the highest average porosity and the grainstone facies have the lowest porosity.

Permeability trends are less straightforward. In the Wolfcamp B2-B1 interval the highest average permeability, 0.20 mD, is found in the grainstone facies. The lowest average permeability is found in the muddy siltstone, calcareous mudstone, and debris flow facies with values ranging from 0.01 mD to 0.1 mD. . In the Wolfcamp A3-A2-A1 and Dean intervals, the highest average permeability is found in the clay rich facies, 0.16-0.60 mD, and the lowest in the sandstone facies, 0.01 mD.

SEM image analysis of pores within each facies made it possible to examine the difference in pore type, size, and connectivity. Most porosity in the silty clay rich facies is due to phyllosilicate framework pores and organic matter pores. Porosity in the carbonate rich facies is due primarily to dissolution porosity. In the lower half of the image in Figure 19, skeletal argillaceous packstone has a clay and organic rich matrix that provides ample locations for phyllosilicate framework pores and organic matter pores. In the upper half of the image, the extensively cemented grainstone contains very little clay or organic matter. Pores are visible only in the small areas containing diagenetic quartz. A high degree of cementation appears to be the primary cause of low porosity and permeability in the grainstone and sandstone facies. Primary porosity and permeability were most likely significantly higher before the pores became occluded by precipitation of carbonate and silica cements. The cement not only shrinks pore size, it also restricts pore connectivity and thus lowers permeability.

Dissolution along carbonate grains and crystals has created some secondary porosity but the secondary pores appear to lack connectivity.

Rock Pyrolysis Data

Total Organic Carbon

Identifying the type and quantity of organic matter in a source rock/reservoir is a crucial step in accurately assessing its hydrocarbon producing potential. The critical parameters related to whether or not a given rock will be a good source rock are the organic richness, the current and past maturity level of the formation, and the organic matter type (Passey et al., 2010). Rock-Eval pyrolysis is an analytical method used to rapidly evaluate these parameters. During Rock-Eval pyrolysis, pulverized samples are gradually heated under an inert atmosphere. This heating distills the free organic compounds (bitumen), then cracks pyrolytic products from the insoluble organic matter (Peters, 1986). This technique provides several measurements (Tissot and Welte, 1984):

TOC = the organic richness of the rock

S1 = the amount of free hydrocarbons (gas and oil) in the sample

S2 = the amount of hydrocarbons generated through thermal cracking of nonvolatile organic matter. S2 is an indication of the quantity of hydrocarbons that the rock has the potential of producing should burial and maturation continue.

S_3 = the amount of CO_2 (in milligrams CO_2 per gram of rock) produced during pyrolysis of kerogen. S_3 is an indication of the amount of oxygen in the kerogen and is used to calculate the oxygen index.

T_{max} = the temperature at which the maximum release of hydrocarbons from cracking of kerogen occurs during pyrolysis (top of S_2 peak). T_{max} is an indication of the stage of maturation of the organic matter.

Core Laboratories conducted Rock-Eval pyrolysis and data analysis. Samples were collected and processed at approximately 10 foot intervals for the Wolfcamp, Lower Leonard, and Spraberry sections of the core. The Dean interval was not sampled. Rock-Eval data for each interval was integrated with a high-resolution facies description in order to establish a relationship between lithofacies, organic richness (TOC) and hydrocarbon generative potential (S2).

In the Wolfcamp B2 and B1 intervals (Table 1), TOC ranges from 0.1 to 6.3 wt. %. The lithofacies with the highest average TOC are those with the highest clay content; silty mudstones (average TOC=4.5) and silty, calcareous, mudstones (average TOC=3.4). The lithofacies with the lowest average TOC is the carbonate rich packstone-grainstone facies (average TOC=1.5). There is a very good correlation between TOC and S2 values; samples with higher levels of TOC have a correspondingly more positive hydrocarbon generative potential. Data plots of measured and calculated parameters provided by Core Laboratories indicate that organic matter is a mixture of Types I and II and that the level of thermal maturity is within the oil window.

In the Wolfcamp A3, A2, and A1 intervals (Table 2), TOC ranges from 0.6 to 8.7 wt. %. As with the lower interval, the clay rich facies have the highest average

TOC and S2 values, the carbonate facies have the lowest TOC and S2 values. Organic matter is a mixture of Types I and II and the rocks are thermally mature.

In the Spraberry interval there are only 2 facies present: silty mudstone with an average TOC of 3.2% and muddy siltstone with an average TOC of 2.7% (Table 3).

Present day organic matter content in these rocks is related to the complex interaction between the rate of primary organic matter production, dilution of organic matter by sediment during deposition, oxygen levels at the water-sediment interface, and the abundance of organic matter consumers. The most organic rich intervals in the core are likely those in which there was a moderate to high level of primary organic matter, moderate dilution by sediment, low to moderate rates of destruction by organisms and where the organic rich sediment was rapidly buried under thick mass gravity flow deposits. This condition is most evident in the Wolfcamp B2 and B1 intervals where TOC values are highest in the mudstone facies just below each debris flow deposit. In the Wolfcamp A3-A2-A1 intervals, a similar pattern is present; however, the mudstone beds are thinner and less abundant. These observations suggest that in the environment in which these rocks were deposited, rapid burial of organic rich sediments had a more important role in preserving organic matter than did anoxia.

Well Log Correlation

Well logging tools are used to measure and define physical rock properties adjacent to the well bore such as lithology, porosity, and permeability. These properties are in turn used to identify potentially productive zones, to determine depth and thickness of these zones, to distinguish between oil, gas, and water in a reservoir, and to estimate hydrocarbon reserves (Asquith and Krygowski, 2004). The Gamma ray (GR) logging tool is one of the most commonly run wireline tools and measures the natural radioactivity in rocks. This tool is especially useful in differentiating clay and organic bearing versus non clay bearing intervals and in correlating geologic formations between wells. Most logging tools have a vertical resolution too low to resolve individual thin beds, thus necessitating the use of drill core or outcrop studies to validate well log interpretations. In this study, the GR and Core GR logs are used to calibrate the core to well logs and to establish a rapid method of recognizing lithofacies associations and in some cases individual rock types. In addition, Core GR values were combined with the core description to calculate an average GR value for each lithofacies (Table 8). The core data were depth shifted to match well log data.

There is a good correlation at the facies scale between the core description and the GR curves (Figures 20 A-D). In the Wolfcamp B2 and B1 intervals it is possible to readily identify the bioclast-lithoclast floatstone facies by its very low GR values and the blocky shape of the curve. Interbedded silty mudstone, muddy siltstone, and skeletal argillaceous packstone are recognized

by a saw-toothed pattern of medium to high GR values. The highest GR values correspond to the most clay and organic rich intervals. There is a gradual, overall GR increase in the B2 and B1 intervals that reflects an increasing mudstone volume. It is not possible to identify those deposits that have undergone slumping.

The transition to the Wolfcamp A3 interval at a depth 8692 feet is marked by a dramatic (left) shift to smaller GR values. This shift represents the onset of the deposition of thin, resedimented carbonate turbidite beds. Individual grainstone beds can sometimes be identified but in general the beds are too thin to be resolved. Moving up through the Wolfcamp A2 and A1 interval, the high frequency oscillatory nature of the GR curve in the A3 section gradually diminishes and the GR curve moves to the right in response to the diminishing thickness and number of grainstone beds. There is a sharp shift to the right in the GR curve at the A2-A1 boundary. Towards the top of A1 there are multiple thick, silty, clay rich intervals that are alternating with thin grainstone, packstone and siltstone beds, a pattern that results in broad fluctuations of the GR curve.

The Dean Formation is composed of siltstone and mudstone intercalated with thick and thin bedded, well cemented sandstone turbidite beds. Sandstone beds are recognized by having very small GR intensities. Thick sandstone beds have a blocky or bulbous shape and thin beds create a distinct cockscomb pattern where they are interbedded with siltstone and mudstone beds.

The rocks described in Core X display a well-defined gamma ray signature that allows for the identification of individual lithofacies and lithofacies associations. Based on comparison to cross sections published by Hamlin and Baumgardner, 2012, this correlation can be extended locally to establish the lateral continuity of vertical facies successions. Further refinement of this correlation is possible by incorporating the entire suite of well logs from Well X.

Summary

The Wolfcamp rocks in Core X were deposited in the Midland Basin during a time when rapid subsidence coincided with highstand conditions. Superimposed on this long term condition are shorter cycles of sea level rise and fall. Maximum carbonate production occurred during highstand periods and resulted in the shedding of large volumes of carbonate clastic debris from platform margin reefs into the basin. During lowstand periods siliciclastic sedimentation was dominant. Low to high levels of bioturbation throughout the core indicate that the bottom water conditions ranged from suboxic to oxic.

The stratigraphic interval represented by Core X contains abundant, thermally mature, organic rich rocks. Relatively low clay content plus the combination of detrital quartz, diagenetic quartz, and biogenic carbonate enhances brittleness by forming a connected network of rigid grains. This rigid network also acts to preserve porosity by sheltering phyllosilicate framework pores during compaction and improves fluid transmissibility during reservoir stimulation by enhancing fracture development. A comparison of the Wolfcamp intervals to other successful source rock/reservoir plays in the United States shows that it has similar mineralogical characteristics (Figure 21). The silty, clay rich facies contain the highest level of TOC, the best porosity, and abundant diagenetic quartz.

Table 9 shows a ranking of reservoir potential for each lithofacies based on average TOC, porosity, and permeability. Lithofacies listed as conventional

reservoirs have sufficient pore volume to store hydrocarbons and enough permeability to allow the flow of oil and gas through the formation. They can be produced at flow rates that produce economic volumes of oil and gas without the use of large stimulation treatments or any special recovery techniques. The muddy siltstone, silty sandstone and skeletal grainstone lithofacies are the only three that rank as possible conventional reservoirs. Unconventional reservoirs are those that cannot be produced at economic flow rates or that do not produce economic volumes of oil and gas without assistance from massive stimulation treatments or special recovery processes and technologies such as horizontal drilling and hydraulic fracturing. The silty mudstone lithofacies ranks highest as a potential unconventional reservoir primarily because of its high TOC content.

The current data set lacks a comprehensive three-dimensional context. Integrating additional core and subsurface data would provide a better understanding of shelf margin to basin development by comparing facies from sedimentary bodies deposited the same time at different locations along the depositional profile.

Figures

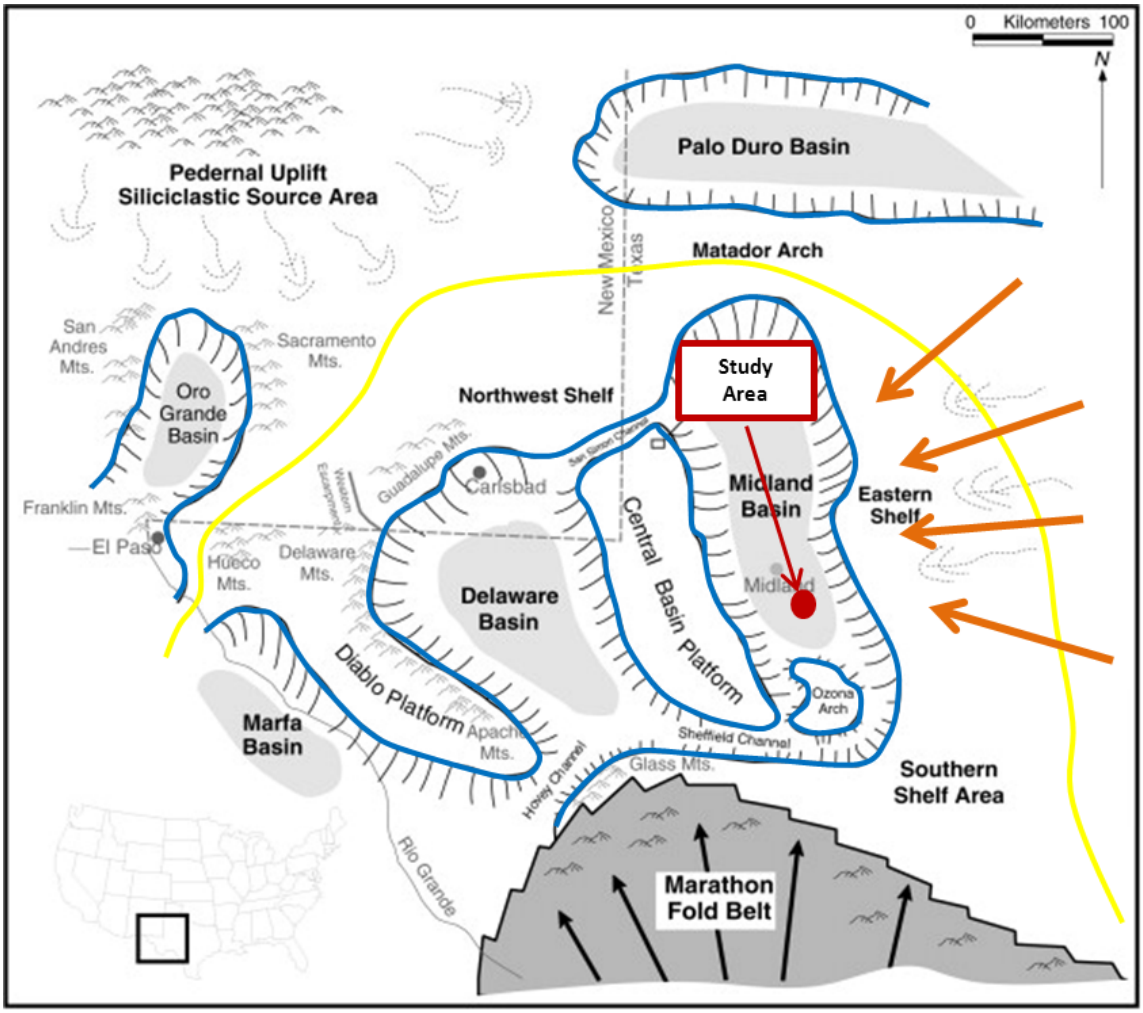

Figure 1: Paleogeography of Permian Basin. The Tabosa Basin, predecessor of the Permian Basin is outlined in yellow. The approximate study area is indicated by the red circle. Carbonate platforms are outlined in blue. Basin locations are light gray. Paleo-wind direction for the Early Permian period is marked by orange arrows.

Modified from Atchley et al., 1999; Adams, 1965; and Soreghan and Soreghan, 2013.

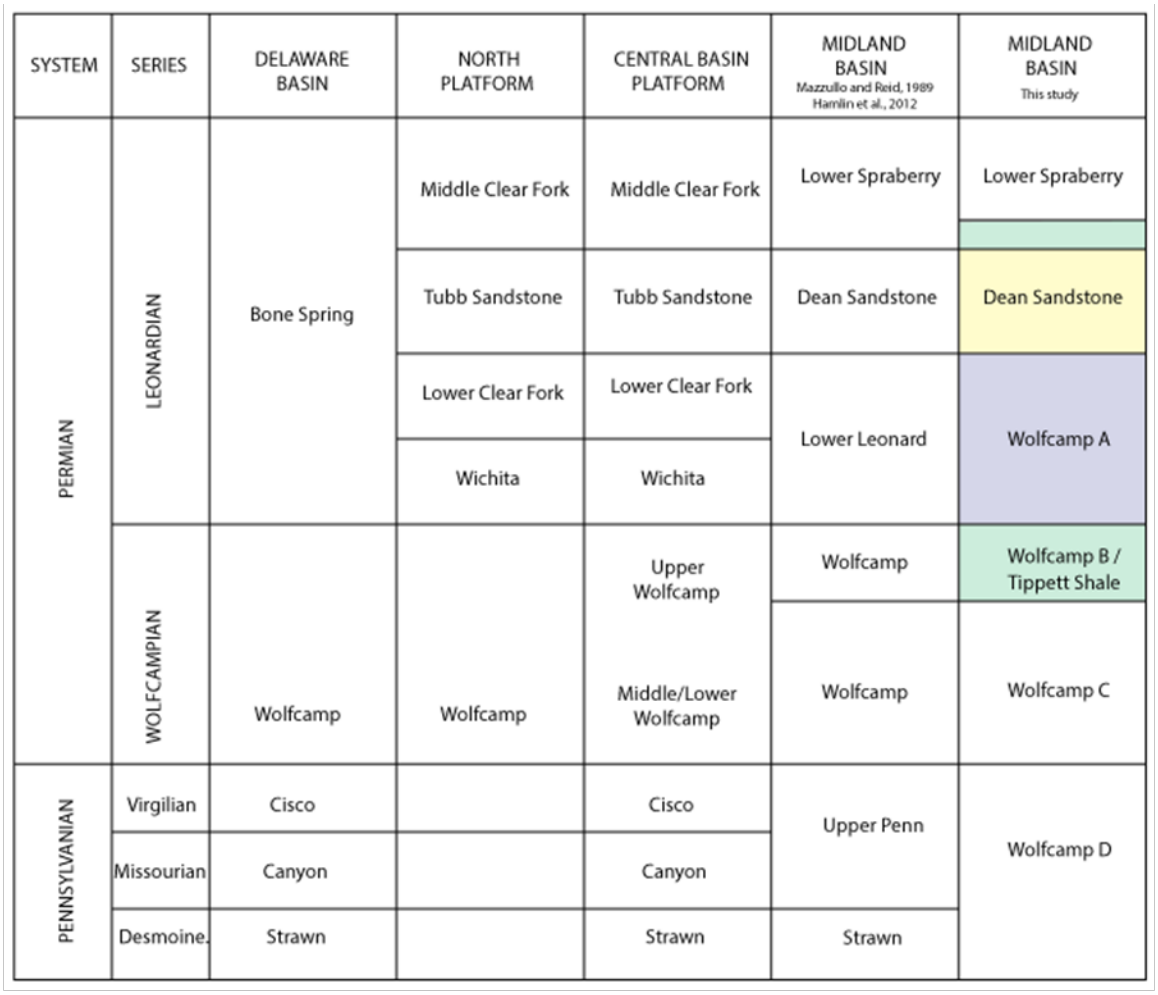

Figure 2: Permian Basin Stratigraphic Column. Colored areas represent intervals covered in this core study.

Sandstone/siltstone

Resedimented carbonate

Mixed siliciclastic/carbonate

Figure 3: Photograph of core, **Wolfcamp B2**, depth 8837-8847 feet. (A) Structureless silty mudstone with phosphatic concretion. (B) Calcareous silty mudstone. (C) Carbonate lithoclast. (D) Ash bed. (E) Carbonate concretion. (F) Skeletal grainstone with erosive base and reworked concretions. (G) Thin, muddy debrite with deformed mudclast. (H) Sheared and rotated package of thin beds at the bottom of a slumped interval, 8847-8843 ft.

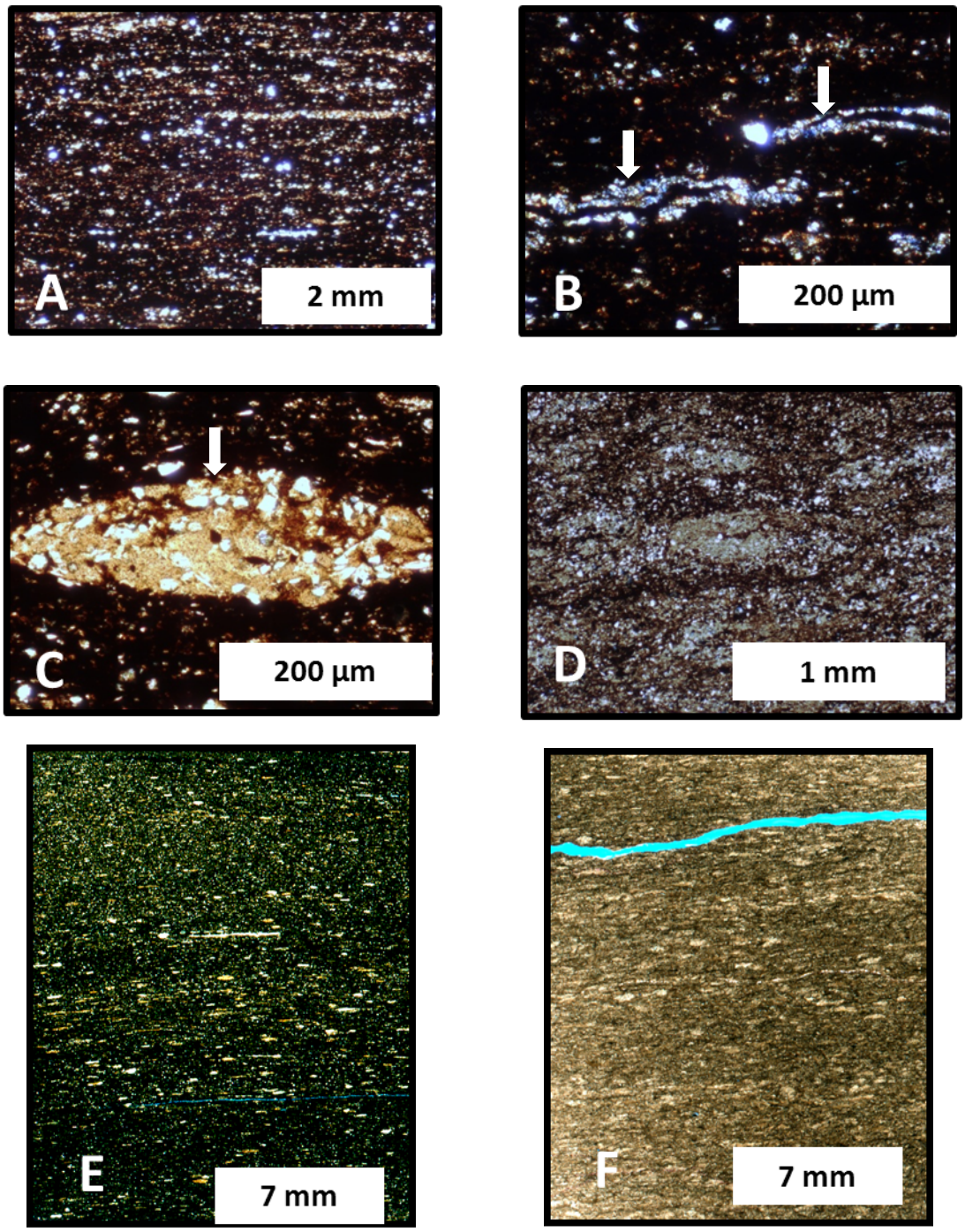

Figure 4: (A) Weakly laminated silty mudstone. (B) Agglutinated benthic foraminifera (white arrows) in silty mudstone. (C) Fecal pellet (white arrow) in silty mudstone. (D) Burrow mottled silty mudstone. (E) Weakly laminated silty mudstone grading upwards to muddy siltstone with fecal pellets and agglutinated benthic foraminifera. (F) Weakly laminated, bioturbated muddy siltstone

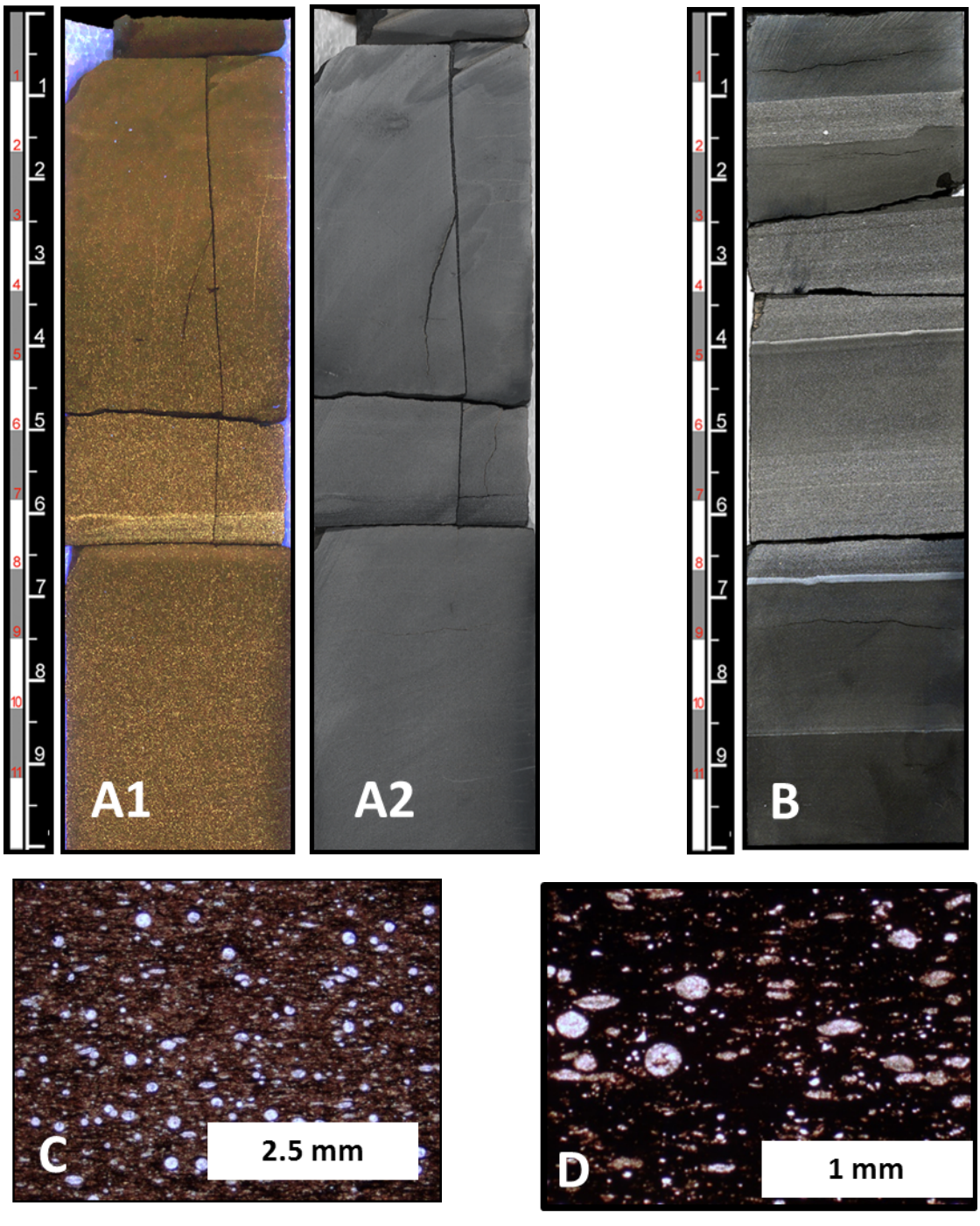

Figure 5: Skeletal argillaceous packstone. (A1) Enhanced UV photo showing two, stacked, graded beds of skeletal argillaceous packstone to wackestone. (A2) Plain light photo of the same sample as A1 showing few discernable features. (B) Thinly interbedded mudstone and skeletal argillaceous packstone. (C and D)Thin section images showing scattered calcispheres (yellow arrow) and benthic foraminifera (red arrow) in a silty, clay rich matrix.

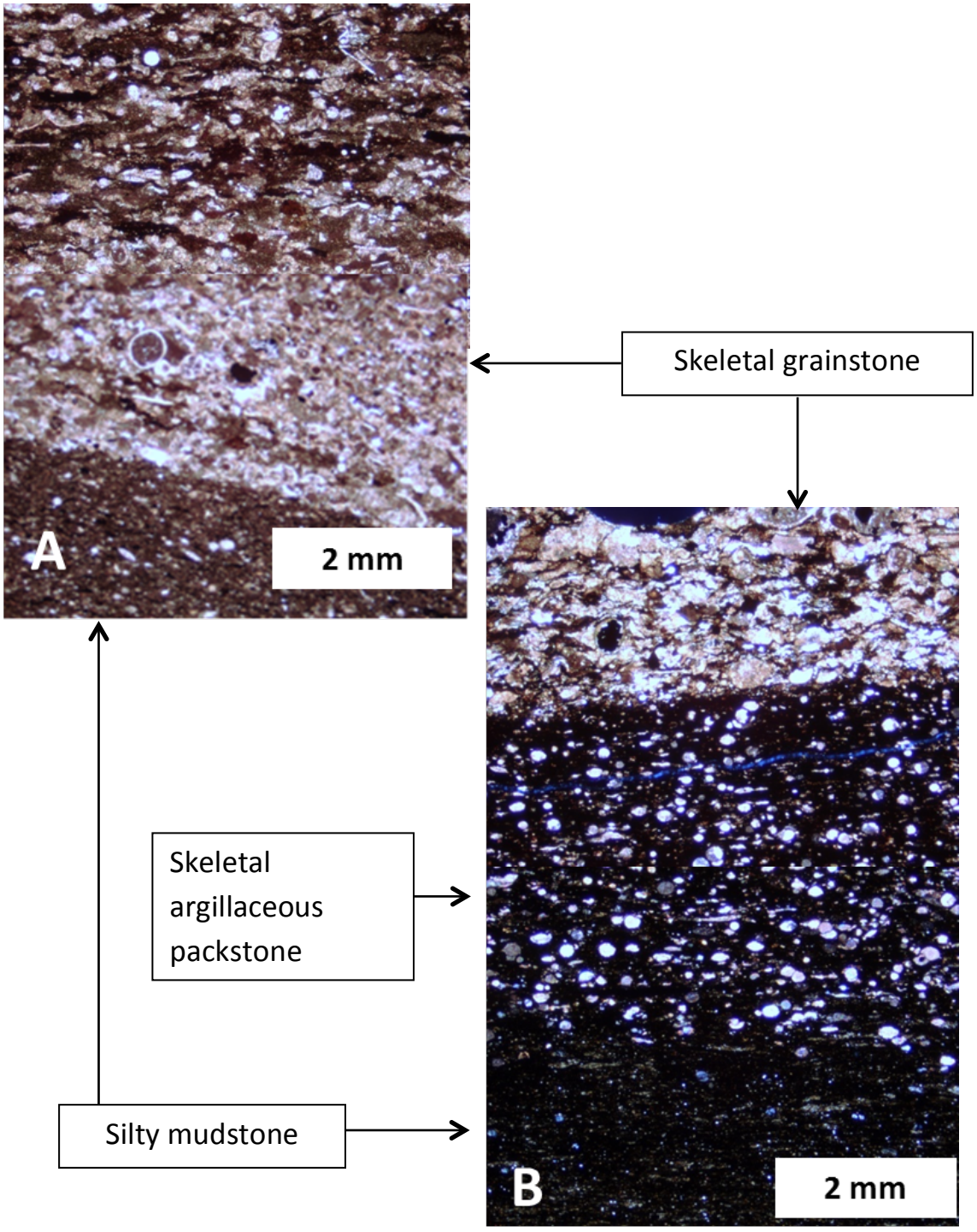

Figure 6: Composite thin section images of skeletal grainstone. (A) Normally graded skeletal grainstone bed overlying silty mudstone. The upper part of the grainstone bed contains abundant flattened mud clasts. (B) Skeletal grainstone bed underlain by skeletal argillaceous packstone. The bottom bed is silty mudstone.

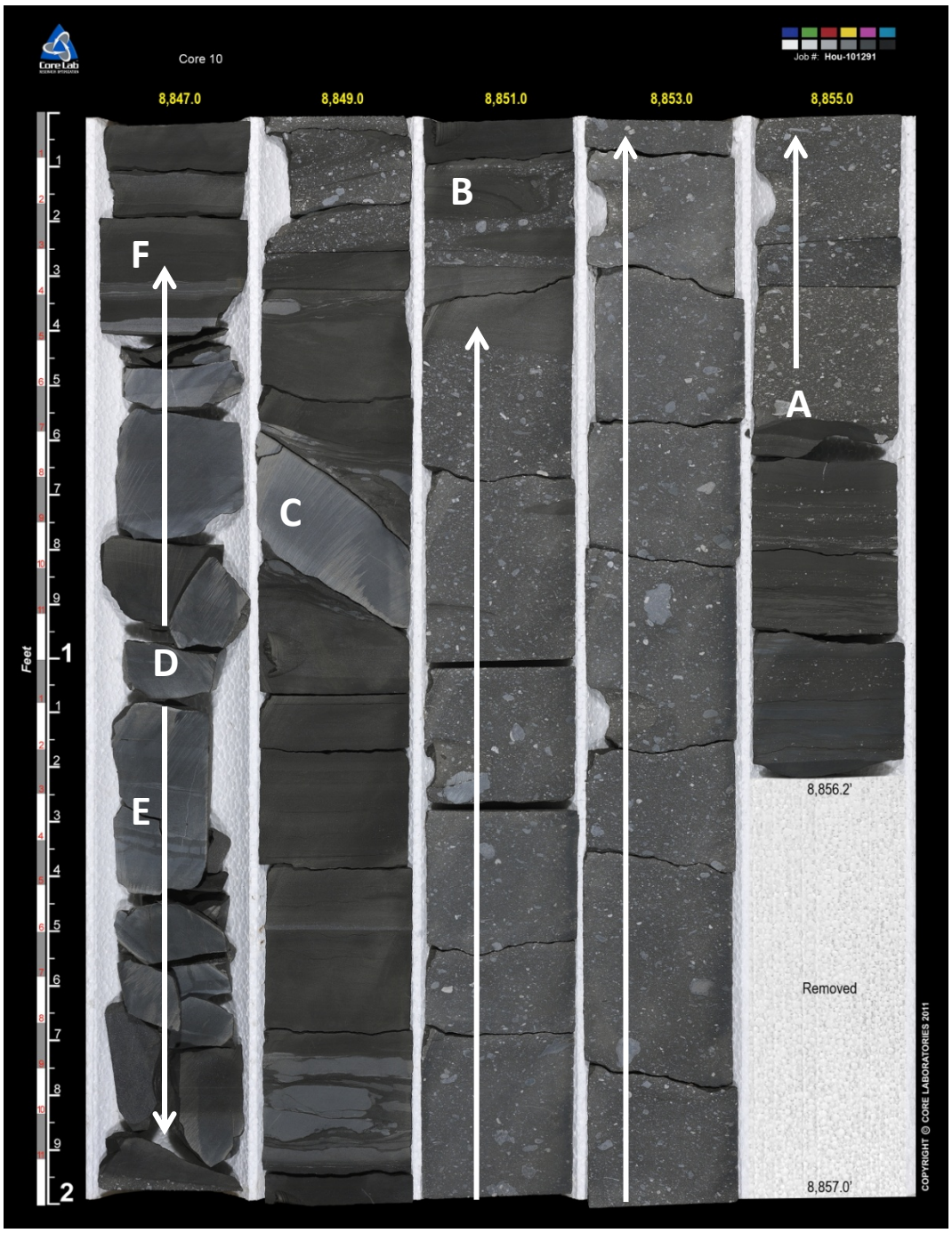

Figure 7: Photograph of core, Wolfcamp **B2**, depth 8837-8847 ft. (A) Thick debris flow deposit with (B) large, internally deformed, flattened mudclasts at top. (C) Rafted carbonate concretion. (D) Slump deposit with (E) extensional structures and (F) sheared thin beds.

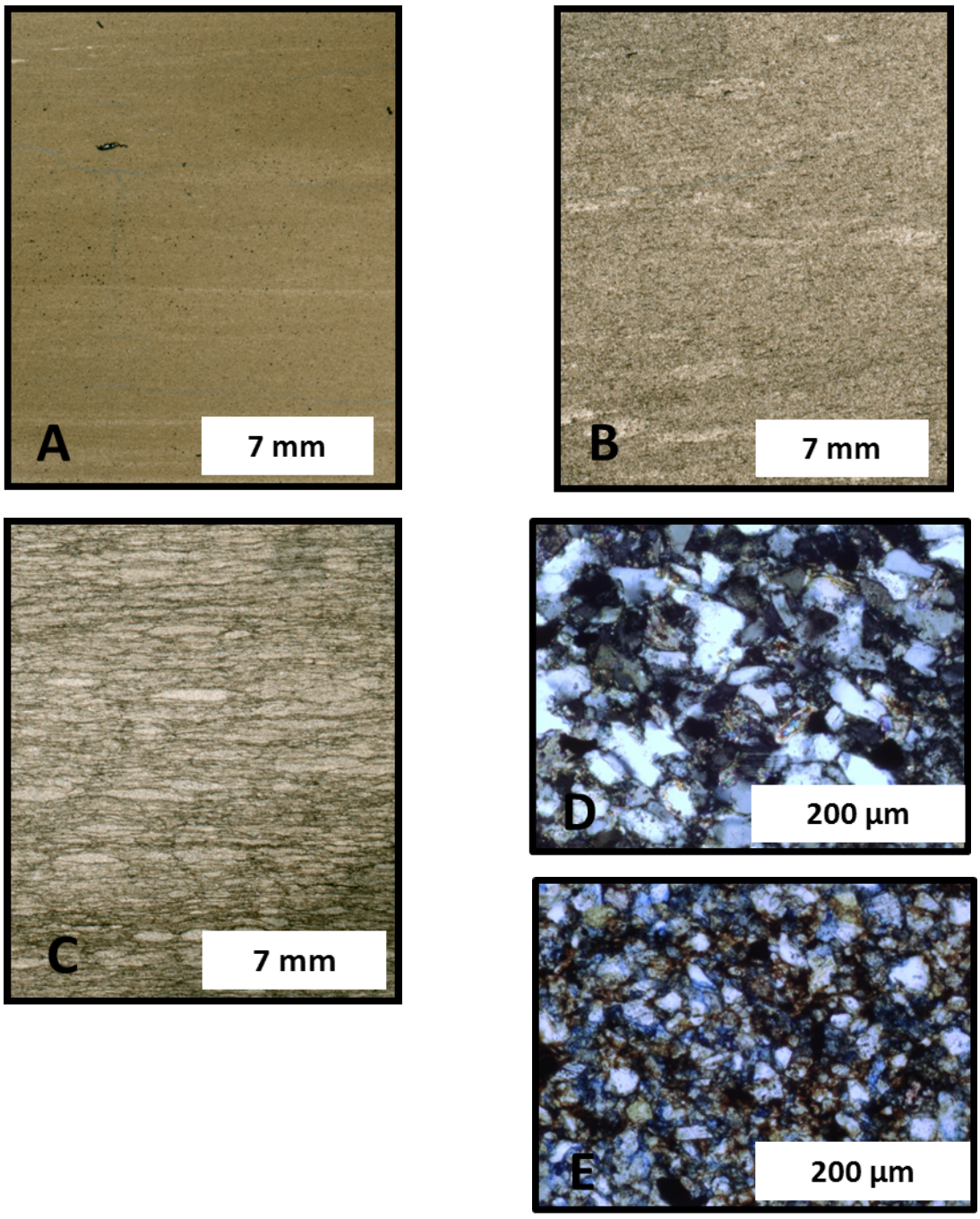

Figure 8: Thin section images of Dean Formation lithofacies: (A) Weakly laminated silty mudstone. (B) Bioturbated siltstone. (C) Bioturbated siltstone. (D) Well cemented, fine grained sandstone. (E) Dolomite and ankerite cemented siltstone.

Figure 9: Photograph of core, Wolfcamp **B1**, depth 8706-8714 ft. (A) Normally graded grainstone (B) Sheared and deformed beds of calcareous silty mudstone and calcareous siltstone. (C) Soft sediment deformation. (D) *Phycosiphon* trace fossils (E) Thinly laminated calcareous silty mudstone with carbonate concretion.

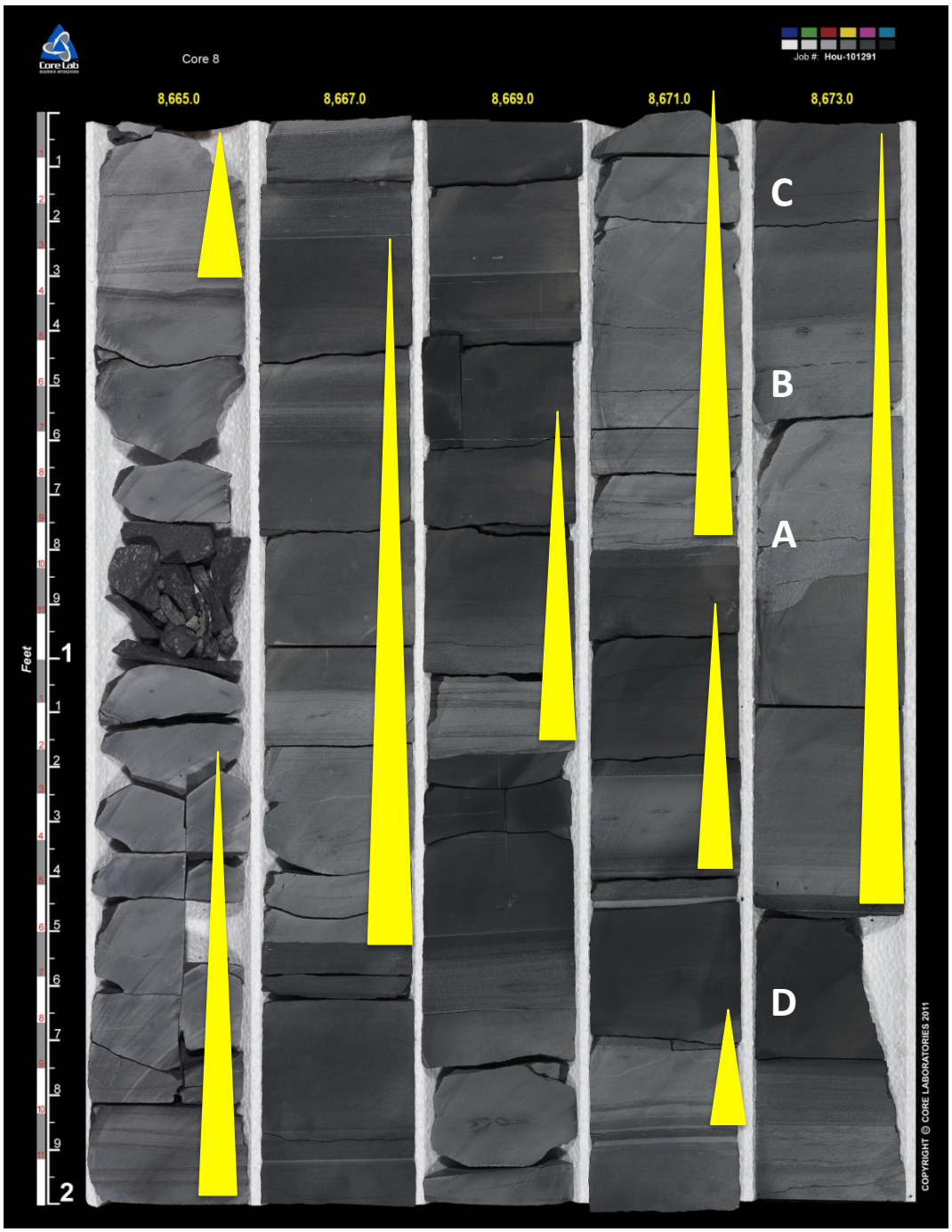

Figure 10: Photograph of core, Wolfcamp **A3**, depth 8665-8675 ft. Stacked, fine grained carbonate turbidites. Yellow markers indicate fining upward packages. (A) Normally graded grainstone with erosive base. (B) Laminated grainstone. (C) Massive packstone. (D) Calcareous silty mudstone.

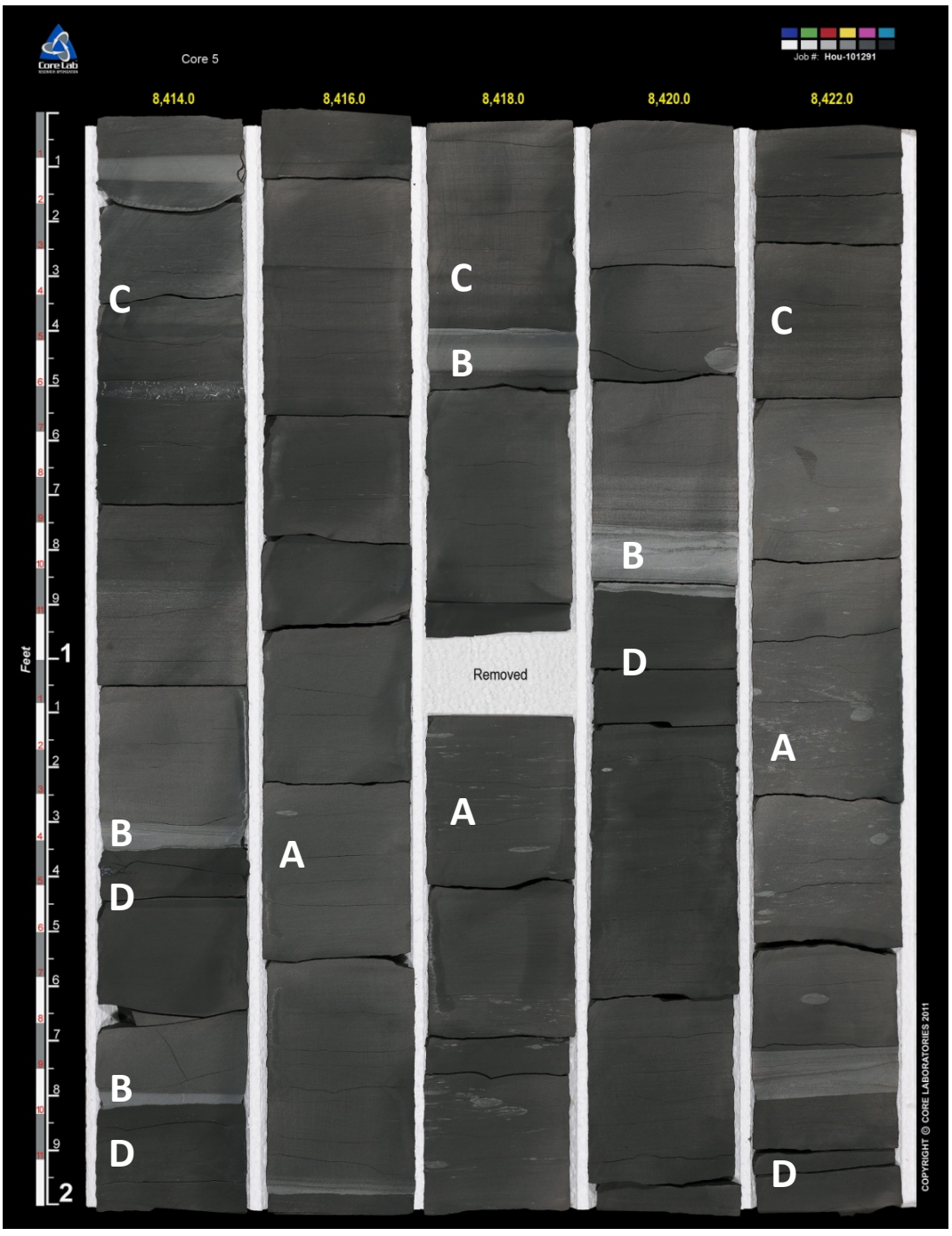

Figure 11: Photograph of core, Wolfcamp **A1**, depth 8414-8424 ft. (A) Bioturbated muddy siltstone with burrows. (B) Thin turbidite beds. (C) Silty mudstone with abundant fecal pellets. (D) Organic rich silty mudstone

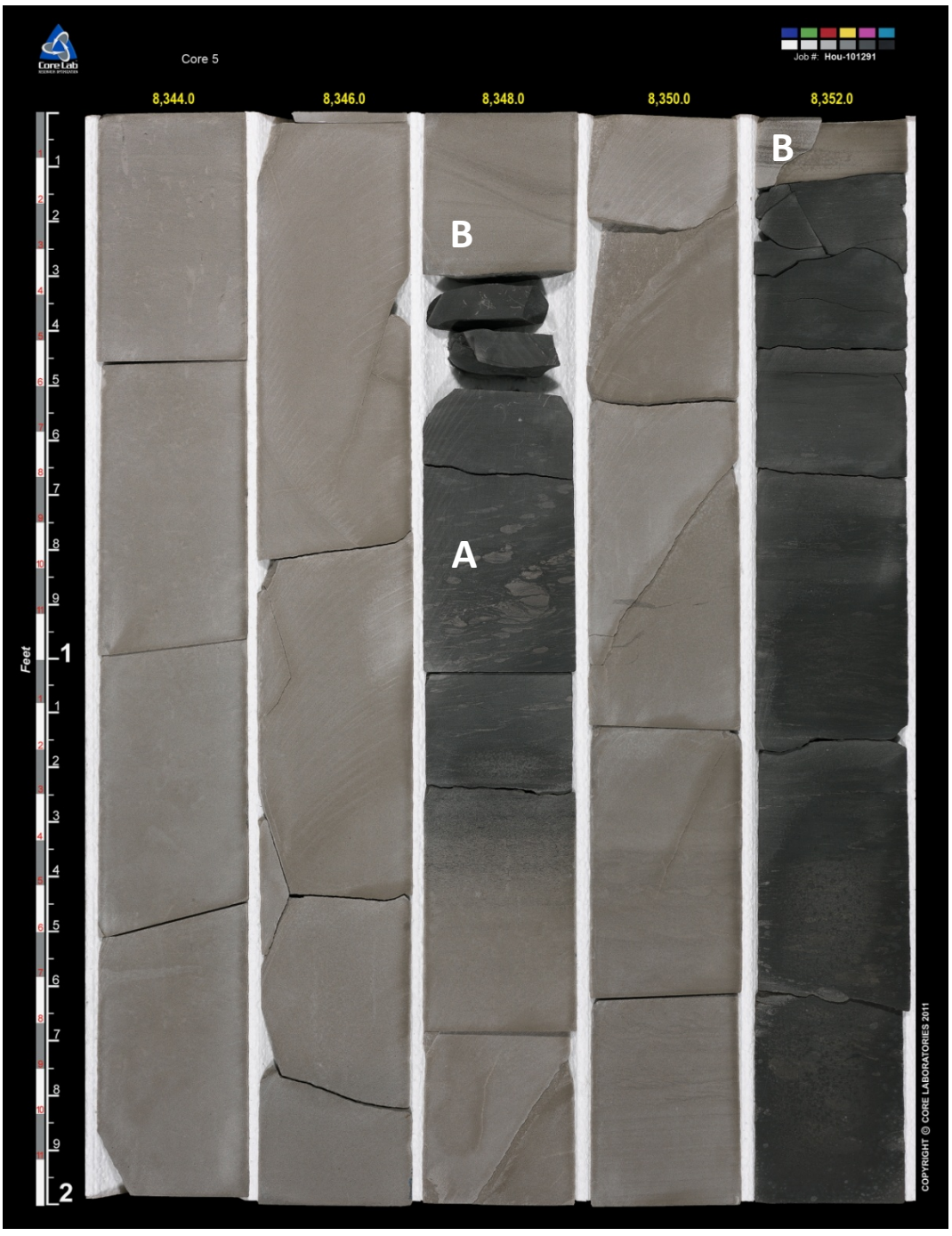

Figure 12: Photograph of core, Dean Formation, depth 8344-8354 ft. (A) Bioturbated, muddy siltstone with burrows. (B) Thick, well cemented, fine grain quartz, turbidite beds.

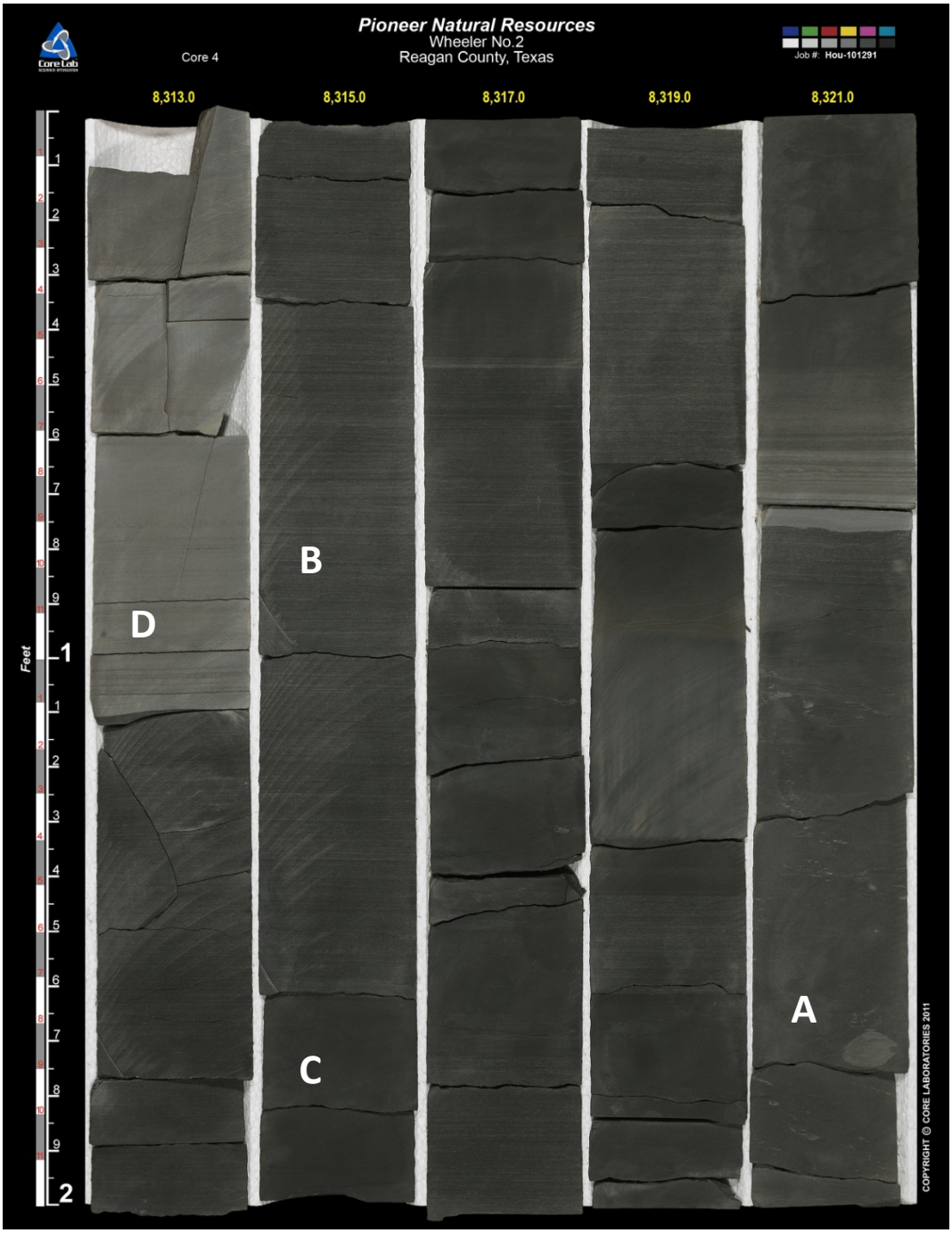

Figure 13: Photograph of core, Dean Formation, depth 8313-8333 ft. (A) Bioturbated, muddy siltstone with burrows. (B) Thinly laminated muddy siltstone. (C) Structureless silty mudstone. (D) Thick, well cemented, fine grain quartz turbidite beds.

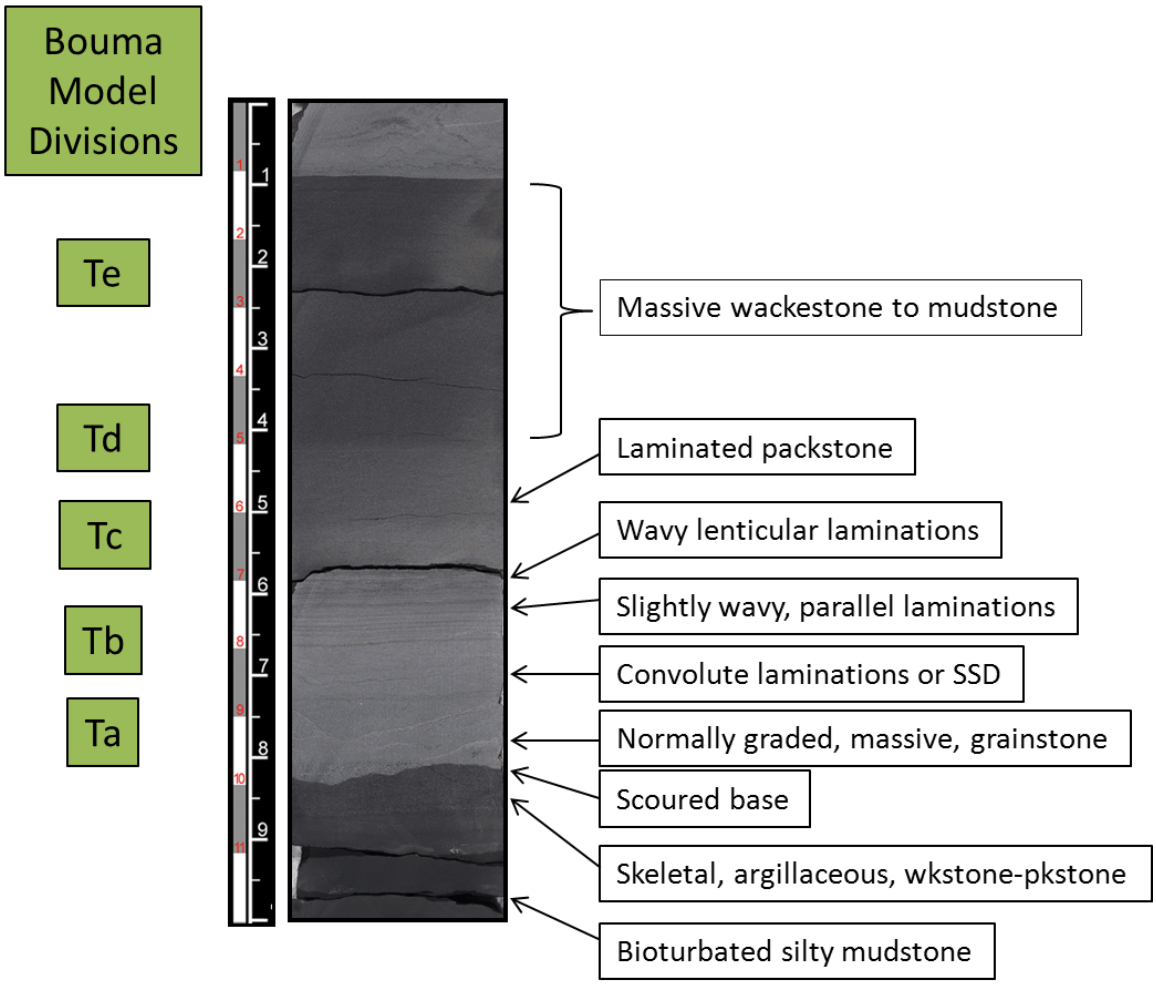

Figure 14: Photograph of core, Wolfcamp **A3**. Fine grained carbonate turbidite bed showing characteristic Bouma Sequence divisions.

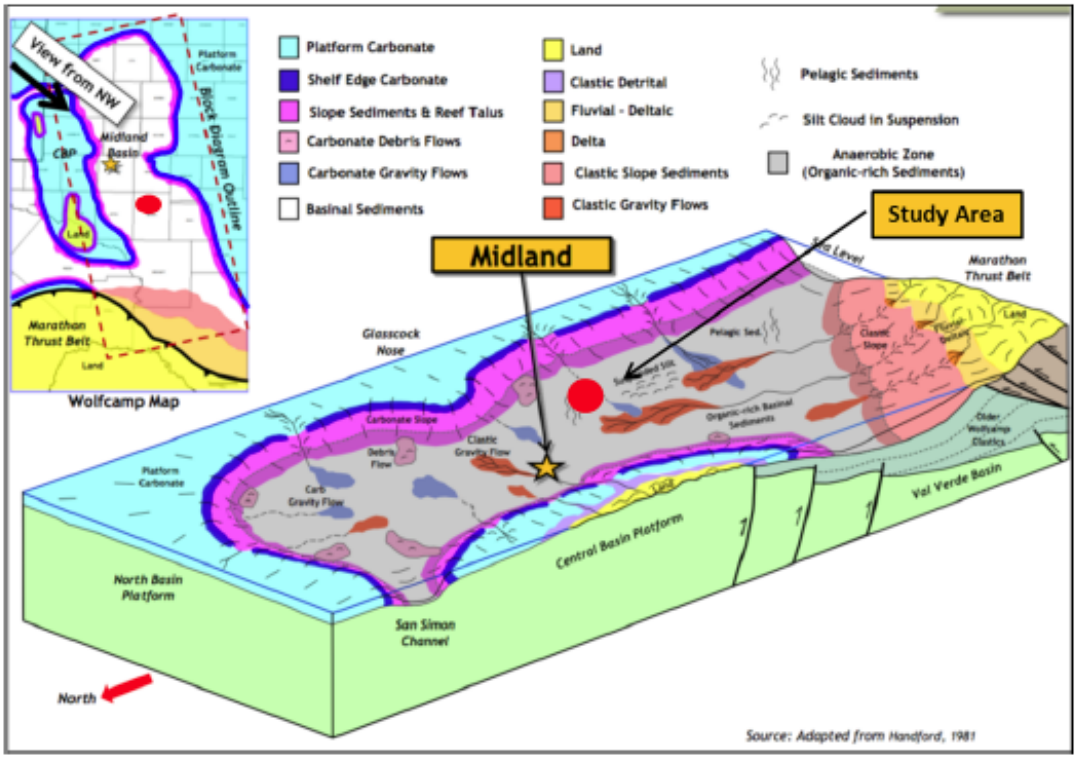

Figure 15: Depositional model for Midland Basin. The relative location of Core X within the basin is indicated by the red circle. The depositional setting is one in which multiple depositional processes are active. These include mass gravity flow, turbidity currents, and suspension settling. Modified from Hanford, 1981; Pioneer Natural Resources Company, 2013.

Series	Stratigraphic Interval	Depositional Processes	Depositional Environment
LEONARDIAN	Spraberry	-Suspension settling -Bottom currents	Basin floor
	Dean	-High density turbidites -Suspension settling -Bottom currents	Basin floor turbidite fan channels and lobes
	A3	-Suspension settling -Bottom currents	Basin floor
	A2	-Medium to high density turbidites -Suspension settling -Bottom currents	Basin floor turbidite fan channels and lobes
	A1		
WOLFCAMPIAN	B2	-Bottom currents -Suspension settling -Low density turbidites -Slumps and slides -Debris flows	Composite wedges formed at the base of platform margin slope and on basin floor
	B1		

Figure 16: Envisioned depositional processes and environments for each stratigraphic interval of Core X

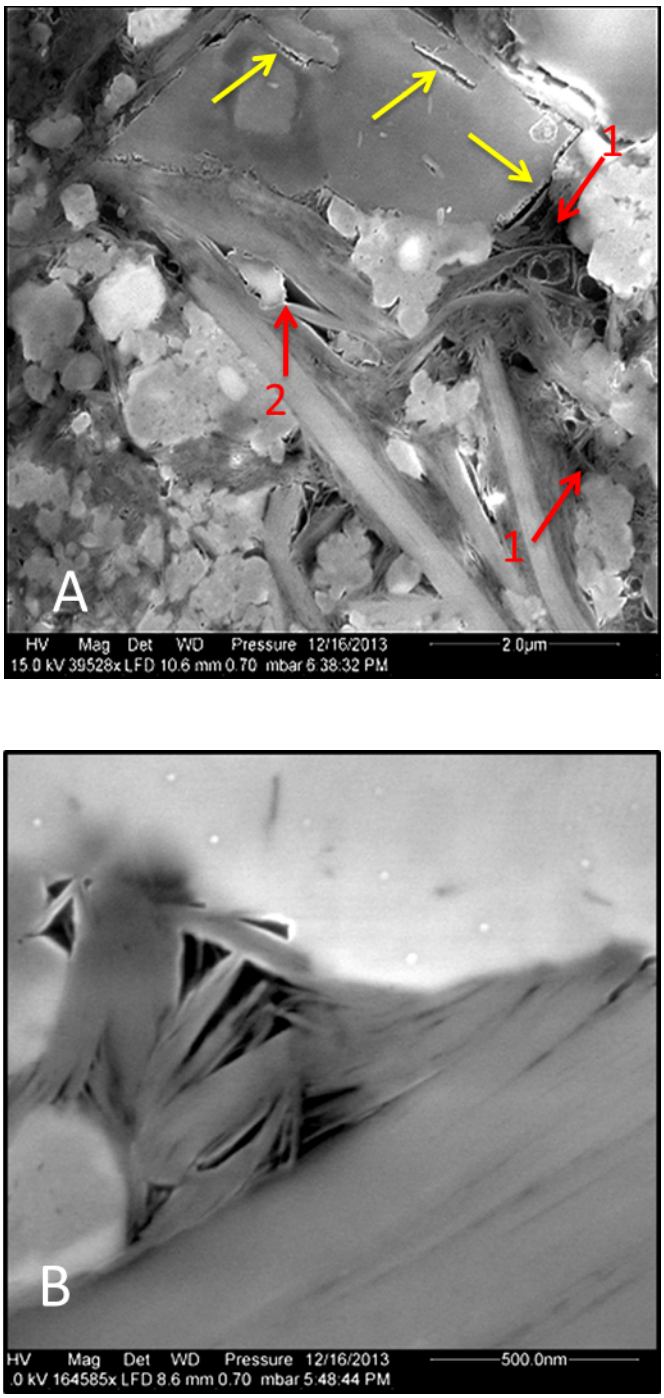

Figure 17: Secondary electron SEM images. (A) Yellow arrows point to dissolution pores within and along the margin of a dolomite grain. Red arrows point to phyllosilicate framework pores in the pressure shadow of the dolomite grain (1) and propped open by diagenetic quartz grain (2). (B) Triangular, edge to face, arrangement of clay flakes create phyllosilicate framework pores.

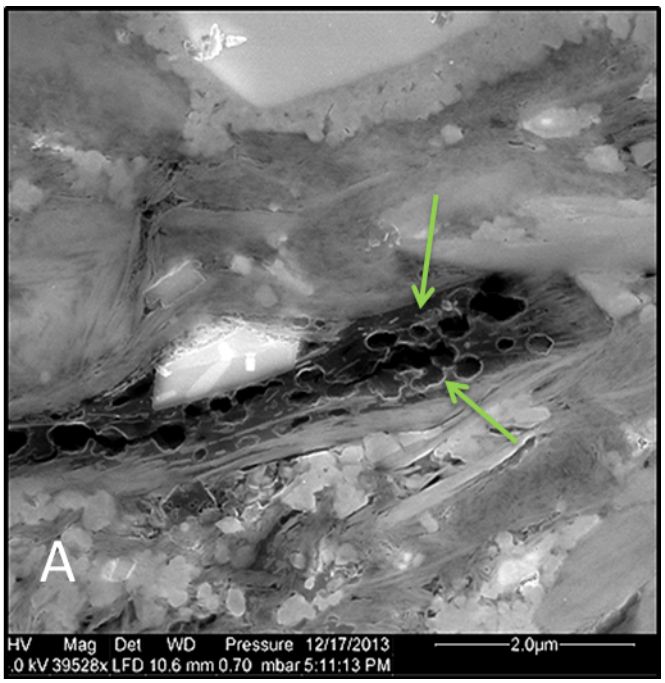

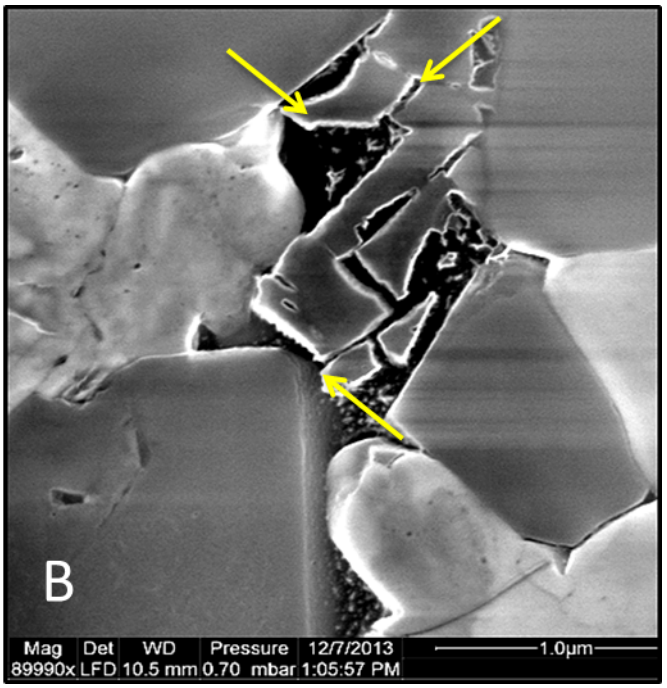

Figure 18: Secondary electron SEM images. (A) Amorphous organic matter (green arrow) with characteristic sponge-like texture of organic matter pores. (B) Hydrocarbon filled pores (yellow arrows) surrounded by diagenetic quartz (light gray) and dolomite (dark gray). Horizontal lines are an image artifact .

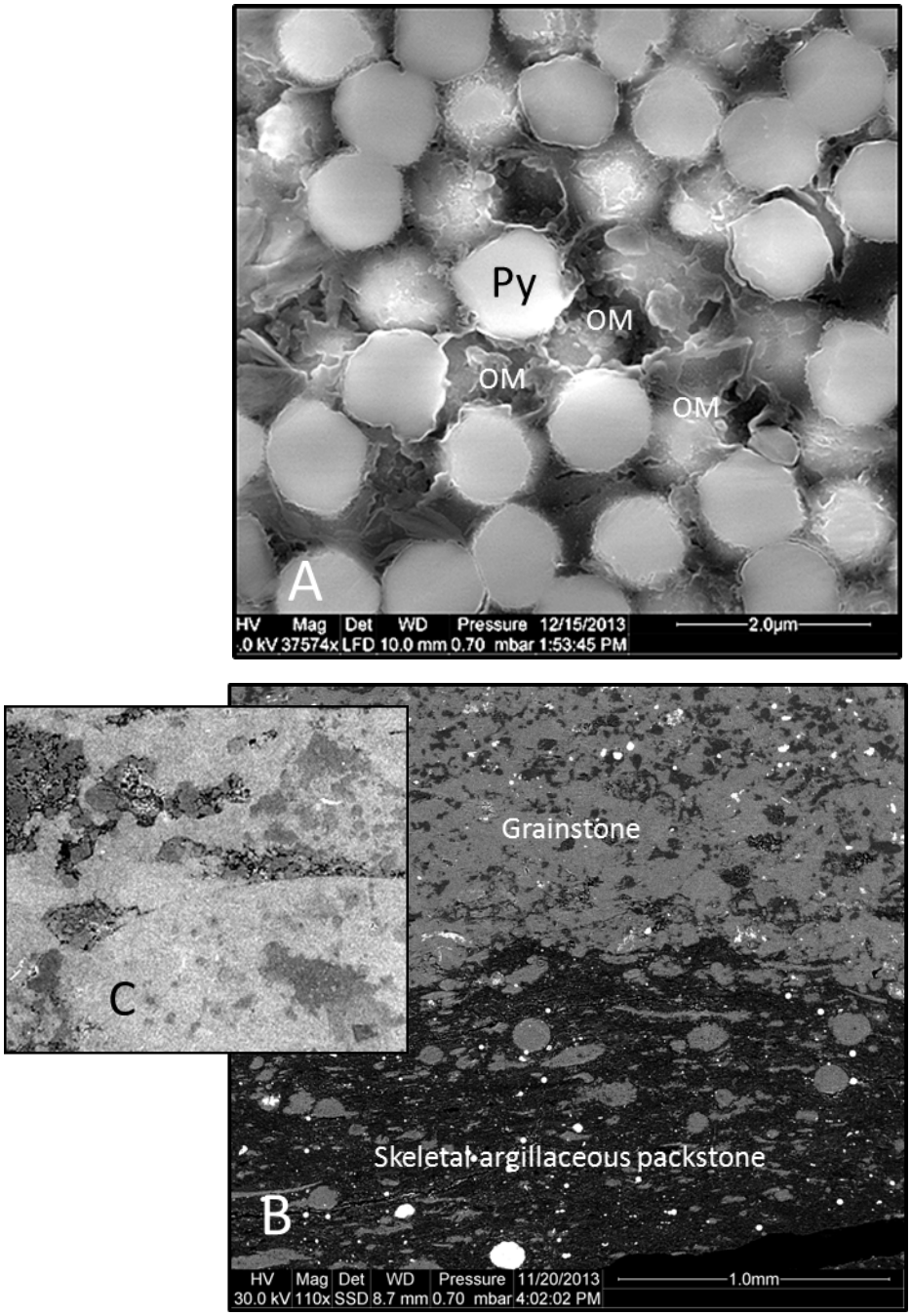

Figure 19: (A) Secondary SEM image; Close up of pyrite framboids where the pores between pyrite grains (Py) are filled with amorphous organic matter (OM). (B) Backscatter SEM image; Wide field of view of the contact between cemented grainstone and skeletal argillaceous packstone. Light gray color indicates carbonate. Dark grey color indicates quartz silt, clay, and organic matter. White indicates pyrite. (C) Close up of grainstone. The black areas in the grainstone are pore spaces almost completely filled with diagenetic quartz.

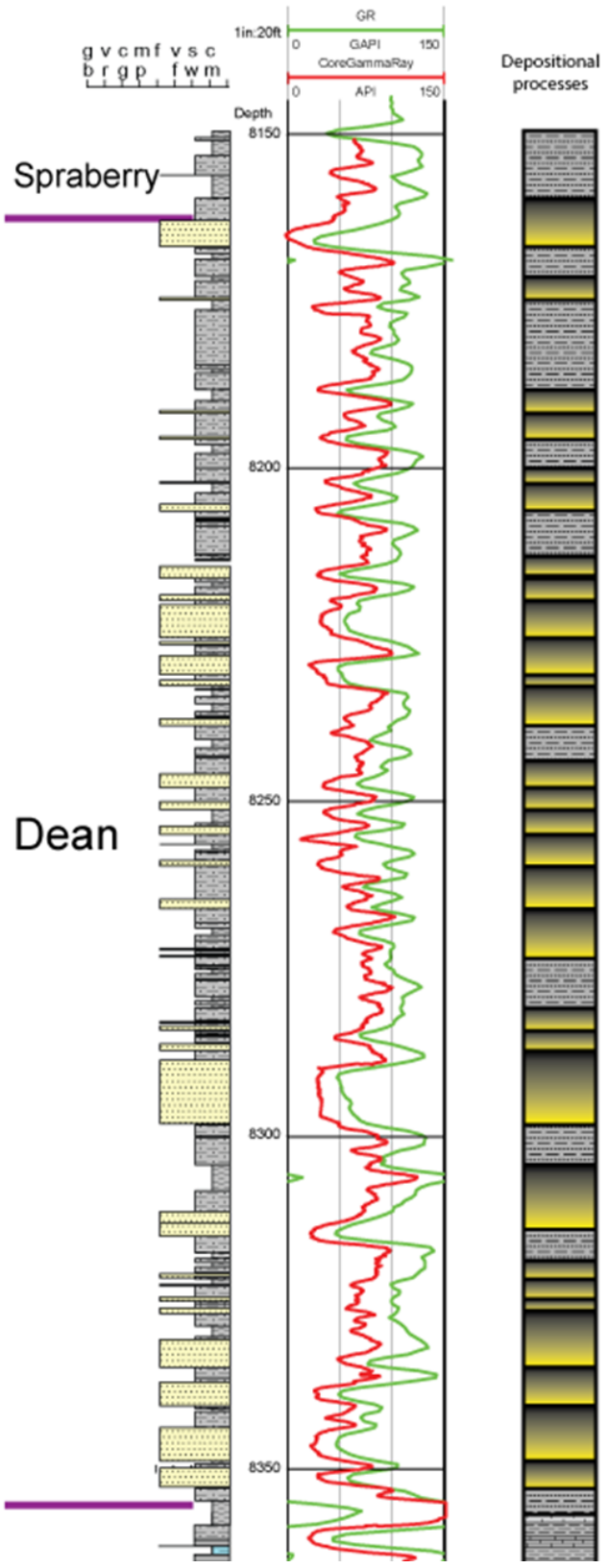

Figure 20A: Lithofacies, gamma ray curves, and inferred depositional processes of Dean and Spraberry. Hemipelagite indicates deposition by suspension settling or bottom currents.

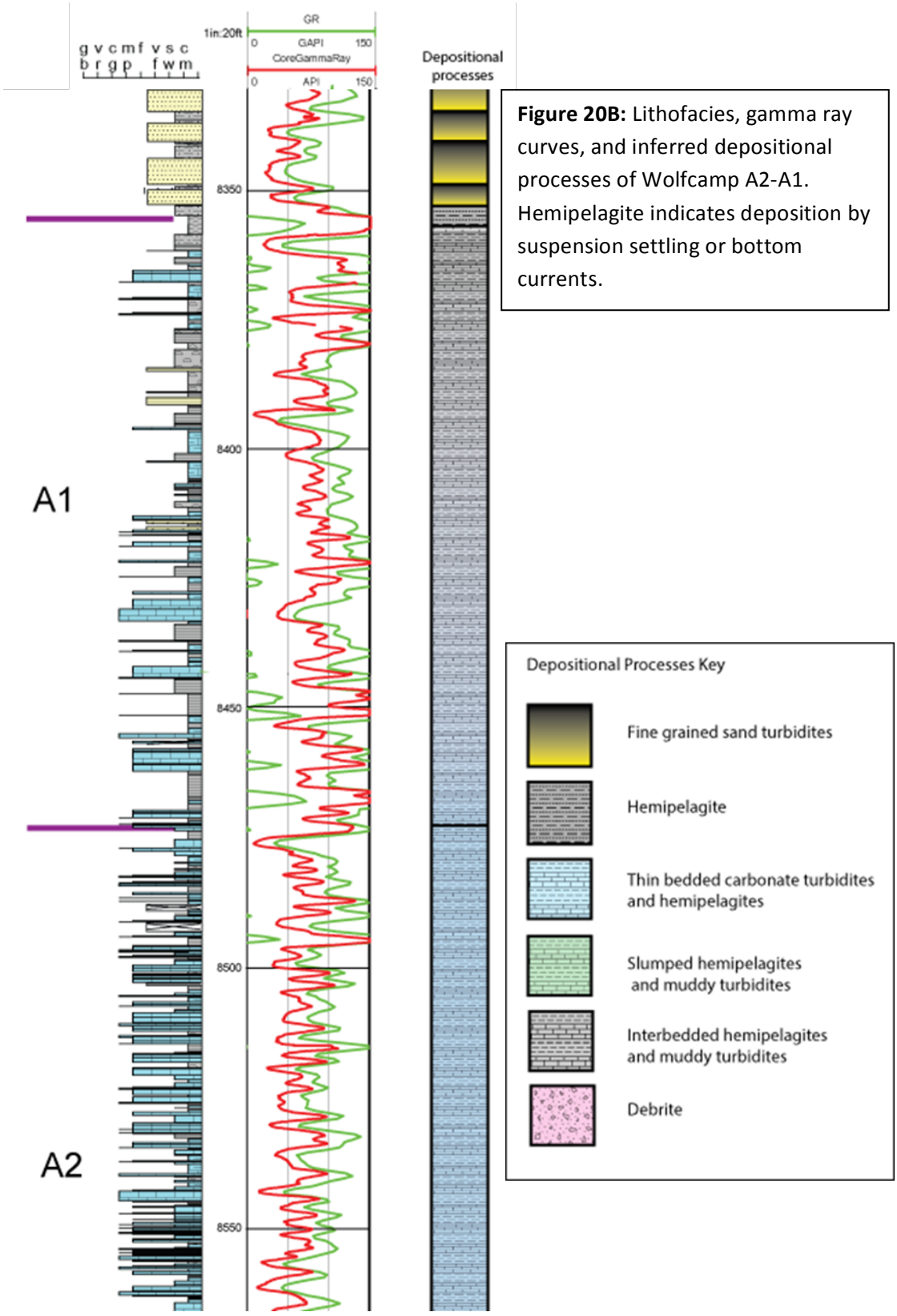

Figure 20B: Lithofacies, gamma ray curves, and inferred depositional processes of Wolfcamp A2-A1. Hemipelagite indicates deposition by suspension settling or bottom currents.

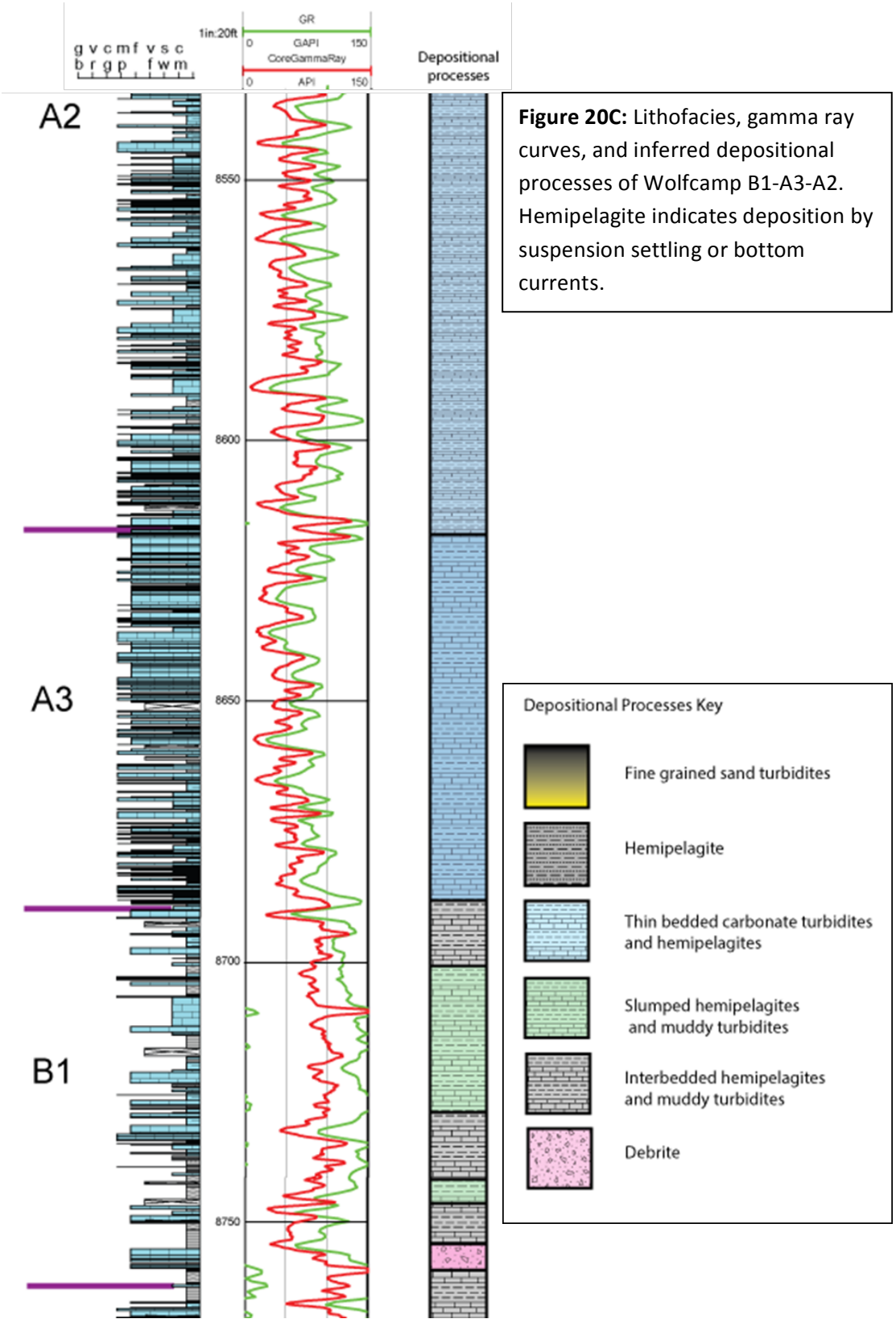

Figure 20C: Lithofacies, gamma ray curves, and inferred depositional processes of Wolfcamp B1-A3-A2. Hemipelagite indicates deposition by suspension settling or bottom currents.

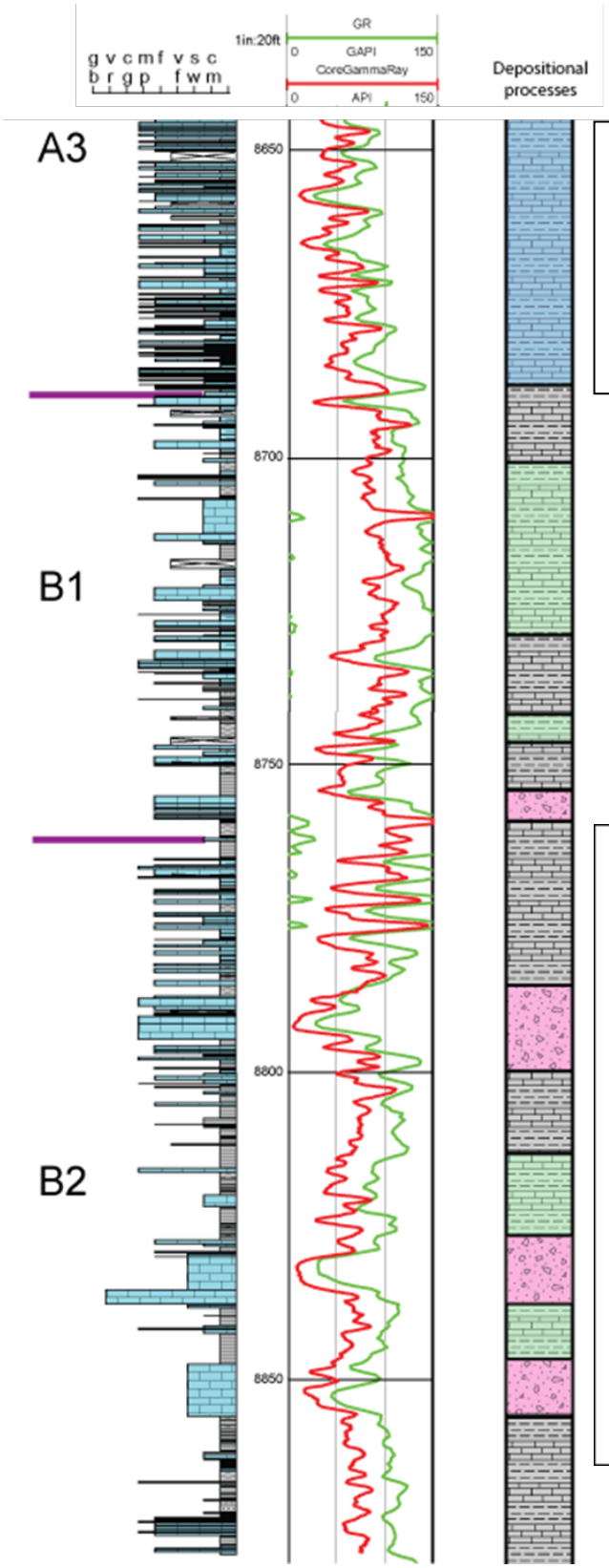

Figure 20D: Lithofacies, gamma ray curves, and inferred depositional processes of Wolfcamp B2-B1. Hemipelagite indicates deposition by suspension settling or bottom currents.

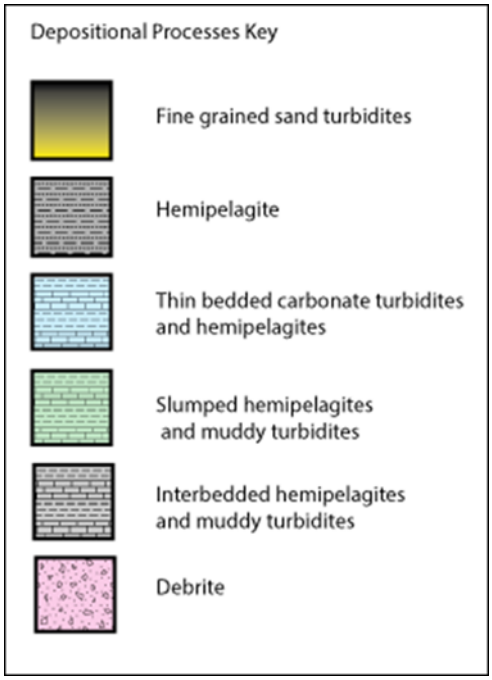

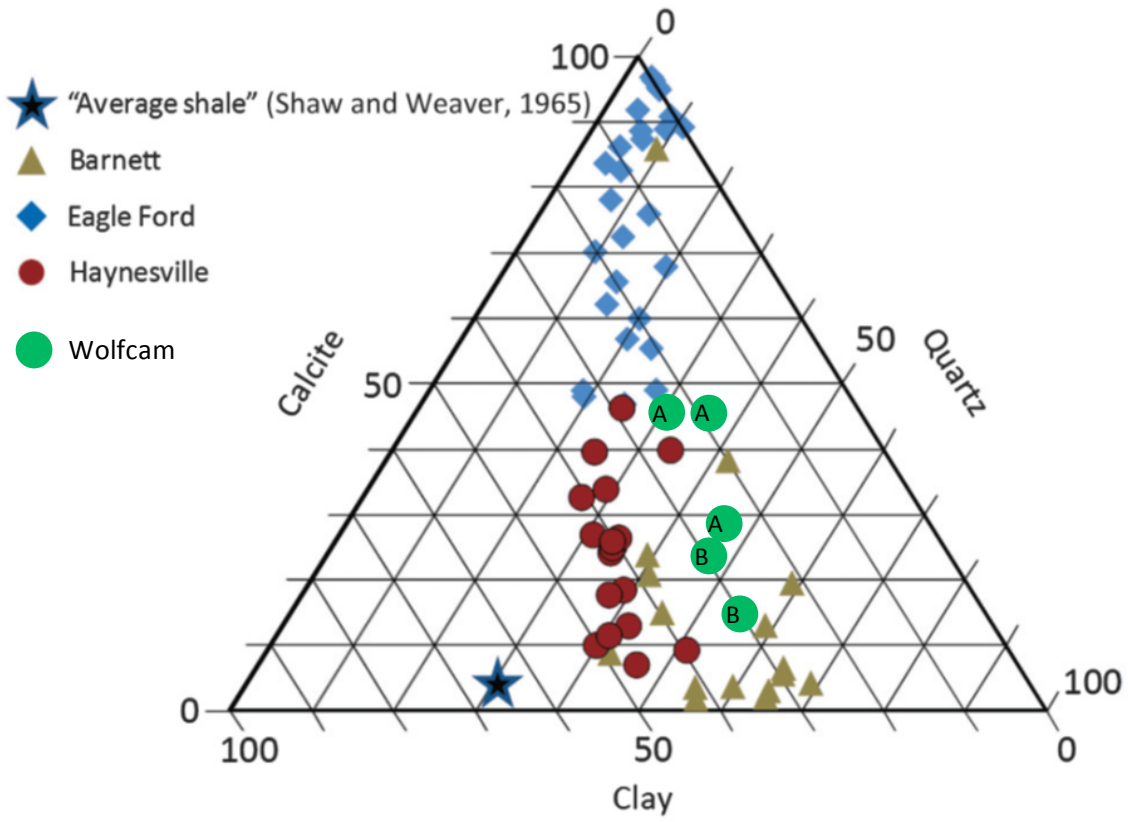

Figure 21: Modified from Hart et al., 2013. Ternary diagram showing compositional variability between four North American source-rock/ reservoir plays. Data points for each of the plays are from a single well in that area. Wolfcamp data is the average for each interval indicated. Note the mineralogic variability that is present between and within plays. The star shows the composition of an "average shale" based on 300 samples (Shaw and Weaver, 1965). Note that most of the data points show less than 50% clay minerals, whereas the clay content of "average shale" is approximately 64%.

Tables

Table 1. TOC Wolfcamp B2-B1

Total organic carbon (%TOC) sorted by facies with total accumulated thickness for each facies, Depth 8692-8876

Facies	Min TOC	Max TOC	Average TOC	Total feet
Silty Mdstn	2.1	6.3	4.5	78
Calc Mdstn	2.0	6.0	3.4	32
Sk-Arg Wk-PK	1.8	4.7	3.2	50
Muddy Sltstn	2.5	4.2	3.1	4
Grainstone	0.1	2.7	1.5	26

Table 2: TOC Wolfcamp A3-A2-A1

Total organic carbon (%TOC) sorted by facies with total accumulated thickness for each facies, Depth 8357-8692

Facies	Min TOC	Max TOC	Average TOC	Total feet
Silty Mdstn	2.3	8.7	4.2	71
Calc Mdstn	1.8	5.2	3.3	60
Sk-Arg Wk-PK	1.5	4.9	3.1	138
Muddy Sltstn	2.3	3.5	3.1	21
Grainstone	0.6	2.3	1.4	37

Table 3: TOC Spraberry

Total organic carbon (%TOC) sorted by facies with total accumulated thickness for each facies, Depth 8148-8165

Facies	Min TOC	Max TOC	Average TOC	Total feet
Silty Mdstn	2.15	4.24	3.2	6.85
Muddy Sltstn	2.15	3.55	2.7	3.25

Table 4: Porosity and Permeability Wolfcamp B2-B1

Average porosity and permeability sorted by facies, Depth 8692-8876

Facies	Average Porosity %	Average Permeability mD
Silty Mdstn	12.0	0.1
Muddy Sltstn	12.6	0.01
Calc Mdstn	11.0	0.01
Sk-Arg Wk-PK	8.3	0.041
Grainstone	2.6	0.20
Debrite	5.6	0.01

Table 5: Porosity and Permeability Wolfcamp A3,A2,A1

Average porosity and permeability sorted by facies, Depth 8357-8692

Facies	Average Porosity %	Average Permeability mD
Silty Mdstn	7.0	0.48
Muddy Sltstn	5.4	0.26
Calc Mdstn	5.3	0.29
Sk-Arg Wk-PK	4.5	0.60
Grainstone	2.8	0.20
Silty Sandstone	2.8	0.007

Table 6: Porosity and Permeability Dean

Average porosity and permeability sorted by facies, Depth 8165-8356

Facies	Average Porosity %	Average Permeability mD
Silty Mdstn	7.4	0.17
Muddy Sltstn	7.2	0.13
Silty Sandstone	6.5	0.01

Table 7: Porosity and Permeability Spraberry

Average porosity and permeability sorted by facies, Depth 8148-8165

Facies	Average Porosity %	Average Permeability mD
Silty Mdstn	3.1	0.89
Muddy Sltstn	7.7	0.03

Table 8: Core Gamma Ray Averages

Average GR values sorted by facies

Facies	Average Core GR Values API
Silty Mdstn	74.5
Muddy Sltstn	71.4
Calc Mdstn	76.6
Sk-Arg Wk-PK	63.7
Grainstone	61.2
Debrite	56.6
Silty Sandstone	55.3

Interval	Lithofacies	Average TOC %	Average Porosity %	Average Permeability mD	Reservoir Potential	
					Conventional	Unconventional
Spraberry	**Silty mudstone**	3.2	3.1	0.89	Not possible	Moderate
	Muddy siltstone	2.7	7.7	0.03	Moderate*	Moderate
Dean	**Silty mudstone**	No data	7.4	0.17	---	---
	Muddy siltstone	No data	7.2	0.13	---	---
	Silty sandstone	2.9[i]	6.5	0.01	Moderate*	---
Wolfcamp A3,A2,A1	**Silty mudstone**	4.2	7.0	0.48	Not possible	High
	Muddy siltstone	3.1	5.4	0.26	Not possible	Moderate
	Silty calcareous mudstone	3.3	5.3	0.29	Not possible	Moderate
	Skeletal argillaceous packstone-wackestone	3.1	4.5	0.6	Not possible	Moderate
	Skeletal grainstone	1.4	2.8	0.20	Poor	Poor
	Silty sandstone	No data	2.8	0.007	Poor*	---
Wolfcamp B1 and B2	**Silty mudstone**	4.5	12.0	0.1	Not possible	High
	Muddy siltstone	3.1	12.6	0.01	Not possible	Moderate
	Silty calcareous mudstone	3.4	11.0	0.01	Not possible	Moderate
	Skeletal argillaceous packstone-wackestone	3.2	8.3	0.041	Not possible	Moderate
	Skeletal grainstone	1.5	2.6	0.20	Poor	Poor
	Bioclast-lithoclast wackestone-floatstone		5.6	0.01	Not possible	

Table 9: Ranking of reservoir potential for lithofacies based on average TOC, porosity, and permeability. Lithofacies rankings for unconventional reservoir potential are relative to one another and apply only to the data set for Core X. Rankings for conventional reservoir potential are based on a combination of data from this study and from other published reports.

* Indicates ranking based on published data

i Average TOC for Dean sandstone from Hamlin et al. 2012

References

Adams, J. E. (1965). Stratigraphic-tectonic development of Delaware Basin. *AAPG Bulletin*, *49*(11), 2140-2148.

Atchley, S. C., Kozar, M. G., & Yose, L. A. (1999). A predictive model for reservoir distribution in the Permian (Leonardian) Clear Fork and Glorieta formations, Robertson Field area, West Texas. *AAPG bulletin*, *83*(7), 1031-1056.

Bagnold, R. A. (1941). The physics of wind blown sand and desert dunes. *Methuen, London*, *265*(10).

Bagnold, R. A. (1954, August). Experiments on a gravity-free dispersion of large solid spheres in a Newtonian fluid under shear. In *Proceedings of the Royal Society of London A: Mathematical, Physical and Engineering Sciences* (Vol. 225, No. 1160, pp. 49-63). The Royal Society.

Berkyova, S., & Munnecke, A. (2010). Calcispheres" as a source of lime mud and peloids–evidence from the early Middle Devonian of the Prague Basin, the Czech Republic. *Bulletin of Geosciences*, *85*(4), 585-602.

Bednarz, M., & McIlroy, D. (2012). Effect of phycosiphoniform burrows on shale hydrocarbon reservoir quality. *AAPG bulletin*, *96*(10), 1957-1980.

Bettis III, A. E. (2012) Climatic and Biotic Controls on Silt Production and Accumulation of Loess. *Nature Education Knowledge* 3(10):25

Bouma, Arnold H. (1962). Sedimentology of some Flysch deposits: A graphic approach to facies interpretation. Elsevier. 168 p.

Bouma, A. H., & Stone, C. G. (Eds.). (2000). *Fine-Grained Turbidite Systems: AAPG Memoir 72* (Vol. 72). AAPG.

Brenchley, P. J., & Newall, G. (1977). The significance of contorted bedding in upper Ordovician sediments of the Oslo region, Norway. *Journal of Sedimentary Research*, *47*(2).

Brown, A. A., & Loucks, R. G. (1993). Influence of sediment type and depositional processes on stratal patterns in the Permian basin-margin Lamar Limestone, McKittrick Canyon, Texas. *MEMOIRS-AMERICAN ASSOCIATION OF PETROLEUM GEOLOGISTS*, 133-133.

Cook, H. E. (1983). Sedimentology of some allochthonous deep-water carbonate reservoirs. *Lower Permian, west Texas: carbonate debris sheets, aprons, or submarine fans*, 442.

Drzewiecki, P. A., & Simó, J. A. (2002). Depositional processes, triggering mechanisms and sediment composition of carbonate gravity flow deposits: examples from the Late Cretaceous of the south-central Pyrenees, Spain. *Sedimentary Geology*, *146*(1), 155-189.

Dunham, R.J. (1962) Classification of carbonate rocks according to depositional texture. *AAPG Memoir 1*. Pp. 108-121.

Dutton, S. P., Flanders, W. A., & Barton, M. D. (2003). Reservoir characterization of a Permian deep-water sandstone, East Ford field, Delaware basin, Texas. *AAPG bulletin*, *87*(4), 609-627.

Dutton, S. P., Kim, E. M., Broadhead, R. F., Raatz, W. D., Breton, C. L., Ruppel, S. C., & Kerans, C. (2005). Play analysis and leading-edge oil-reservoir development methods in the Permian basin: Increased recovery through advanced technologies. *AAPG bulletin*, *89*(5), p.553-576.

Dutton, S. P. (2008). Calcite cement in Permian deep-water sandstones, Delaware Basin, west Texas: Origin, distribution, and effect on reservoir properties. *AAPG bulletin*, *92*(6), 765-787.

Einsele, G. (1992). *Sedimentary basins: evolution, facies, and sedimentary budget*. Springer-Verlag.

Faugeres, J.C., Stowe, D.A.V. (1993. Bottom-current-controlled sedimentation: a synthesis of the contourite problem. Sedimentary Geology, V.82, p. 287-297

Fertl, W., & Chilingar, G. (1988). Total organic carbon content determined from well logs. *SPE formation evaluation*, *3*(2), 407-419.

Fischer, A. G., & Sarnthein, M. (1988). Airborne silts and dune-derived sands in the Permian of the Delaware Basin. *Journal of Sedimentary Research*, *58*(4).

Flèugel, E., & Munnecke, A. (2010). *Microfacies of carbonate rocks: analysis, interpretation and application*. Springer.

Frenzel, H. N., et al., 1988, The Permian basin region, *in* L. L. Sloss, ed., Sedimentary cover—North American craton; U.S.:Boulder, Colorado, Geological Society of America, The Geology of North America, V. D-2, p. 261– 306.

Fu, Qilong (2011). A synthesis of the Wolfcampian platform carbonate system in the Permian Basin Region. Bureau of Economic Geology, The University of Texas at Austin

Gentry, M. D. (2003). Applications of artificial neural networks in the identification of flow units, Happy Spraberry Field, Garza County, Texas. *Master's thesis, Texas A&M University. Texas A&M University. Available electronically from http://hdl. handle. net/1969*, *1*, 1604.

Ghadeer, S. G., & Macquaker, J. H. (2011). Sediment transport processes in an ancient mud-dominated succession: a comparison of processes operating in marine offshore settings and anoxic basinal environments. *Journal of the Geological Society*, *168*(5), 1121-1132.

Gillette, D. A. (1977). Fine particulate emissions due to wind erosion [to total soil movement]. *Transactions of the ASAE [American Society of Agricultural Engineers]*.

Hamlin, H.S. (2010). Depositional and diagenetic controls on reservoir quality, Spraberry and Dean Sandstones, Northern Midland Basin; *Seminar*,*Bureau of Economic Geology, University of Texas at Austin.*

Hamlin, H. S., & Baumgardner, R. W. (2012). Wolfberry (Wolfcampsian-Leonardian) Deep-water Depositional Systems in the Midland Basin: Stratigraphy, Lithofacies, Reservoirs, and Source Rocks. *Bureau of Economic Geology, University of Texas at Austin.*

Hampton, M. A. (1972). The role of subaqueous debris flow in generating turbidity currents. *Journal of Sedimentary Research*, *42*(4)

Handford, C.R. (1981). Sedimentology and Genetic Stratigraphy of Dean and Spraberry Formations (Permian), Midland Basin, Texas. Bureau of Economic Geology, University of Texas at Austin.

Hart, B. S., Macquaker, J. H., & Taylor, K. G. (2013). Mudstone ("shale") depositional and diagenetic processes: Implications for seismic analyses of source-rock reservoirs. *Interpretation*, *1*(1), B7-B26.

Hills, J. M. (1972). Late Paleozoic sedimentation in west Texas Permian basin. *AAPG Bulletin*, *56*(12), 2303-2322.

Hobson, J. P., Caldwell, C. D., & Toomey, D. F. (1985). Early Permian deep-water allochthonous limestone facies and reservoir, west Texas. *Am. Assoc. Pet. Geol., Bull.;(United States)*, *69*(12).

Janson, X., Kerans, C., Bellian, J. A., & Fitchen, W. (2007). Three-dimensional geological and synthetic seismic model of Early Permian redeposited basinal carbonate deposits, Victorio Canyon, west Texas. *AAPG bulletin*, *91*(10), 1405-1436.

Kocurek, G., & Kirkland, B. L. (1998). Getting to the source: aeolian influx to the Permian Delaware basin region. *Sedimentary Geology*, *117*(3), 143-149.

Lewis, K.B. (1971). Slumping on a continental slope inclined at 1°-4°. *Sedimentology*, 16, p. 97-110.

Loucks, R. G., & Ruppel, S. C. (2007). Mississippian Barnett Shale: Lithofacies and depositional setting of a deep-water shale-gas succession in the Fort Worth Basin, Texas. *AAPG bulletin*, *91*(4), 579-601.

Loucks, R. G., Reed, R. M., Ruppel, S. C., & Hammes, U. (2012). Spectrum of pore types and networks in mudrocks and a descriptive classification for matrix-related mudrock pores. *AAPG bulletin*, *96*(6), 1071-1098.

Lowe, D. R. (1982). Sediment gravity flows: II Depositional models with special reference to the deposits of high-density turbidity currents. *Journal of Sedimentary Research*, *52*(1).

McCave, I. N. (1972). Transport and escape of fine-grained sediment from shelf areas. *IN: SHELF SEDIMENT TRANSPORT: PROCESS AND PATTERN*.

Macquaker, J. H., Bentley, S. J., & Bohacs, K. M. (2010). Wave-enhanced sediment-gravity flows and mud dispersal across continental shelves: Reappraising sediment transport processes operating in ancient mudstone successions. *Geology*, *38*(10), 947-950.

Marszalek, D. S. (1975). Calcisphere ultrastructure and skeletal aragonite from the alga Acetabularia antillana. *Journal of Sedimentary Research*, *45*(1).

Mazzullo, S. J. (1980). Calcite pseudospar replacive of marine acicular aragonite, and implications for aragonite cement diagenesis. *Journal of Sedimentary Research*, *50*(2).

Mazzullo, S. J. (1981). Facies and burial diagenesis of a carbonate reservoir: Chapman Deep (Atoka) field, Delaware Basin, Texas. *AAPG Bulletin*, *65*(5), 850-865.

Mazzullo, S. J. (1982). Stratigraphy and depositional mosaics of lower Clear Fork and Wichita Groups (Permian), northern Midland basin, Texas. *AAPG Bulletin*, *66*(2), 210-227.

Mazzullo, S. J. (1995). Permian Stratigraphy and Facies, Permian Basin (Texas—New Mexico) and Adjoining Areas in the Midcontinent United States. In *The Permian of Northern Pangea* (pp. 41-60). Springer Berlin Heidelberg.

Mazzullo, S. J. (1997). Permian. *AAPG bulletin*, *81*(10), 1750-1753.

Mazzullo, S. J. (1998). Stratigraphic architecture of Lower Permian, cyclic carbonate reservoirs (Chase Group) in the Mid-Continent USA, based on outcrop studies. *AAPG bulletin*, *82*(3), 464-483.

Mazzullo, S. J. (2004). Overview of porosity evolution in carbonate reservoirs. *Kansas Geological Society Bulletin*, *79*(1/2), 20-28.

Mazzullo, S. J., & Cys, J. M. (1979). Marine aragonite sea-floor growths and cements in Permian phylloid algal mounds, Sacramento Mountains, New Mexico. *Journal of Sedimentary Research*, *49*(3).

Mazzullo, S. J., Mazzullo, J., & Harris, P. M. (1985). Significance of Eolian Quartzose Sheet Sands on Emergent Carbonate Shelves: Permian of West Texas-New Mexico: ABSTRACT. *AAPG Bulletin*, *69*(2), 284-284.

Mazzullo, S. J., & Harris, P. M. (1991). An overview of dissolution porosity development in the deep-burial environment, with examples from carbonate reservoirs in the Permian Basin. *Permian Basin Plays–Tomorrow's Technology Today: West Texas Geological Society, Publ*, (91-89), 125-138.

Mazzullo, S.J., Reid,A.M. (1989). Lower Permian Platform and Basin Depositional Systems, Northern Midland Basin, Texas. *SEPM Special Publication No.44.*

Middleton, G. V., & Hampton, M. A. (1973). Part I. Sediment gravity flows: mechanics of flow and deposition.

Milliken, K., Choh, S. J., Papazis, P., & Schieber, J. (2007). "Cherty" stringers in the Barnett Shale are agglutinated foraminifera. *Sedimentary Geology*, *198*(3), 221-232.

Milliken, K. L., Rudnicki, M., Awwiller, D. N., & Zhang, T. (2013). Organic matter–hosted pore system, Marcellus Formation (Devonian), Pennsylvania. *AAPG bulletin*, *97*(2), 177-200.

Monicard, R. P. (1980). Properties of Reservoir Rocks—Core Analysis: Houston, Gulf Publishing Company, 168 p.

Montgomery, Scott, L., (1996). Permian "Wolfcamp" Limestone Reservoirs: Powell Ranch Field, Eastern Midland Basin, *AAPG Bulletin*, V. 80, No. 9, P.1349-1365

Moretti, M., & Sabato, L. (2007). Recognition of trigger mechanisms for soft-sediment deformation in the Pleistocene lacustrine deposits of the Sant'Arcangelo Basin (Southern Italy): Seismic shock vs. overloading. *Sedimentary Geology*, *196*(1), 31-45.

Mulder, T., & Alexander, J. (2001). The physical character of subaqueous sedimentary density flows and their deposits. *Sedimentology*, *48*(2), 269-299.

Mullins, H. T., & Cook, H. E. (1986). Carbonate apron models: alternatives to the submarine fan model for paleoenvironmental analysis and hydrocarbon exploration. *Sedimentary Geology*, *48*(1), 37-79.

Mutti, E. & Ricci Lucci, F. (1975) Turbidite facies and facies associations. In: Examples of turbidite facies and associations from selected formations of the northern Apennines. IX Int. Congress of Sedimentology, Field Trip A-11, p. 21-36.

Owen, G., Moretti, M., & Alfaro, P. (2011). Recognising triggers for soft-sediment deformation: Current understanding and future directions. *Sedimentary Geology*, *235*(3), 133-140.

Page, L. R., & Adams, J. E. (1940). Stratigraphy, Eastern Midland Basin, Texas. *AAPG Bulletin*, *24*(1), 52-64.

Passey, Q. R., Creaney, S., Kulla, J. B., Moretti, F. J., & Stroud, J. D. (1990). A practical model for organic richness from porosity and resistivity logs. *AAPG Bulletin*, *74*(12), 1777-1794.

Passey, Q. R., Dahlberg, K. E., Sullivan, K., Yin, H., Brackett, B., Xiao, Y., & Guzman-Garcia, A. G. (2006). *Petrophysical Evaluation of Hydrocarbon Pore-thickness in Thinly Bedded Clastic Reservoirs: AAPG Archie Series, No. 1* (No. 1). Aapg.

Passey, Q., Bohacs, K., Esch, W., Klimentidis, R., & Sinha, S. (2010, June). From oil-prone source rock to gas-producing shale reservoir-geologic and petrophysical characterization of unconventional shale gas reservoirs. In *International Oil and Gas Conference and Exhibition in China*.

Pemberton, S. G., MacEachern, J. A., Gingras, M. K., & Saunders, T. D. (2008). Biogenic chaos: Cryptobioturbation and the work of sedimentologically friendly organisms. *Palaeogeography, Palaeoclimatology, Palaeoecology*, *270*(3), 273-279.

Reading, H.G., Richards, M. (1994). Turbidite systems in deep-water basin margins classified by grain size and feeder system. *AAPG Bulletin*, 78, pp. 792-822.

Reid, A. M., Reid, S. T., Mazzullo, S. J., & Robbins, S. T. (1988). Revised fusulinid biostratigraphic zonation and depositional sequence correlation, subsurface Permian basin. *AAPG (Am. Assoc. Pet. Geol.) Bull.;(United States)*, *72*(CONF-8802107-).

Ross, C. A., & Ross, J. R. (1995). Foraminiferal zonation of late Paleozoic depositional sequences. *Marine Micropaleontology*, *26*(1), 469-478.

Ross, C. A., & Ross, J. R. (1994). Permian sequence stratigraphy and fossil zonation.

Ross, C. A., & Ross, J. R. (1995). Foraminiferal zonation of late Paleozoic depositional sequences. *Marine Micropaleontology*, *26*(1), 469-478.

Ruppel, S. C., & Ward, W. B. (2013). Outcrop-based characterization of the Leonardian carbonate platform in west Texas: Implications for sequence-stratigraphic styles in the Lower Permian. *AAPG bulletin*, *97*(2), 223-250.

Sagri, M. (1979). Upper Cretaceous carbonate turbidites of the Alps and Apennines deposited below the calcite compensation level. *Journal of Sedimentary Research*, *49*(1).

Saller, A. H., Dickson, J. A. D., & Boyd, S. A. (1994). Cycle stratigraphy and porosity in Pennsylvanian and Lower Permian shelf limestones, eastern Central Basin Platform, Texas. *AAPG bulletin*, *78*(12), 1820-1842.

Schmitt, G. T. (1954). Genesis and depositional history of Spraberry Formation, Midland basin, Texas. *AAPG Bulletin*, *38*(9), 1957-1978.

Scholle, P. A., & Ulmer-Scholle, D. (2003). AAPG Memoir 77, Chapter 3: GRAINS: Skeletal Fragments: Other Micro-and Nannofossils.

Silver, B. A., & Todd, R. G. (1969). Permian cyclic strata, northern Midland and Delaware basins, west Texas and southeastern New Mexico. *AAPG Bulletin*, *53*(11), 2223-2251.

Schieber, J., Krinsley, D., & Riciputi, L. (2000). Diagenetic origin of quartz silt in mudstones and implications for silica cycling. *Nature*, *406*(6799), 981-985.

Schieber, J., Southard, J., & Thaisen, K. (2007). Accretion of mudstone beds from migrating floccule ripples. *Science*, *318*(5857), 1760-1763.

Schieber, J. (2009). Discovery of agglutinated benthic foraminifera in Devonian black shales and their relevance for the redox state of ancient seas. *Palaeogeography, Palaeoclimatology, Palaeoecology*, *271*(3), 292-300.

Schieber, J., & Southard, J. B. (2009). Bedload transport of mud by floccule ripples—Direct observation of ripple migration processes and their implications. *Geology*, *37*(6), 483-486.

Schieber, J., Southard, J. B., & Schimmelmann, A. (2010). Lenticular shale fabrics resulting from intermittent erosion of water-rich muds—interpreting the rock record in the light of recent flume experiments. *Journal of Sedimentary Research*, *80*(1), 119-128.

Schieber, J. (2010, February). Common themes in the formation and preservation of intrinsic porosity in shales and mudstones-illustrated with examples across the Phanerozoic. In *SPE Unconventional Gas Conference*.

Schieber, J. (2011). Reverse engineering mother nature—shale sedimentology from an experimental perspective. *Sedimentary Geology*, *238*(1), 1-22.

Schieber, J. (2013) SEM Observations on ion-milled samples of Devonian black shales from Indiana and New York: The petrographic context of multiple pore types. In: (W Camp, E Diaz, B Wawak, eds.), *Electron Microscopy of Shale Hydrocarbon Reservoirs*; *AAPG Memoir* **102**, 153-171.

Schlager, W., Reijmer, J. J., & Droxler, A. (1994). Highstand shedding of carbonate platforms. *Journal of Sedimentary Research*, *64*(3).

Shanmugam, G. (2000). 50 years of turbidite paradigm (1950s-1990s): deep-water processes and facies models-a critical perspective. *Marine and Petroleum Geology*, 17 no. 2, 285-342

Slatt, R. M., & O'Brien, N. R. (2011). Pore types in the Barnett and Woodford gas shales: Contribution to understanding gas storage and migration pathways in fine-grained rocks. *AAPG bulletin*, *95*(12), 2017-2030.

Soreghan, G. S., & Soreghan, M. J. (2013). Tracing Clastic Delivery to the Permian Delaware Basin, USA: Implications For Paleogeography and Circulation In Westernmost Equatorial Pangea. *Journal of Sedimentary Research*, *83*(9), 786-802.

Stowe, D.A., Howell, D.G., Nelson, C.H. (1985). Sedimentary, tectonic, and sea-level controls. *Submarine fans and related turbidite systems*, Springer Verlag, New York

Stowe, D.A., & Mayall, M. (2000). Deep-water sedimentary systems: new models for the 21st century. *Marine and Petroleum Geology 17*, no. 2 (2000): 125-135

Talling, P. J., Masson, D. G., Sumner, E. J., & Malgesini, G. (2012). Subaqueous sediment density flows: Depositional processes and deposit types. *Sedimentology*, *59*(7), 1937-2003.

Tappan, H., and Loeblich, AR. (1988). Foraminiferal Evolution, Diversification, and Extinction. *Journal of Paleontology*, Vol. 62, Issue 5, 695-714.

Tissot, B.P., and Welte, D.H., 1984. *Petroleum Formation and Occurrence* (2nd ed.): Heidelberg (Springer-Verlag)

Tsoar, H., & Pye, K. (1987). Dust transport and the question of desert loess formation. *Sedimentology*, *34*(1), 139-153.

Tucker, M. E., & Wright, V. P. (2009). *Carbonate sedimentology*. Wiley.

Ward, R. F., Kendall, C. G. S. C., & Harris, P. M. (1986). Upper Permian (Guadalupian) facies and their association with hydrocarbons--Permian basin, west Texas and New Mexico. *AAPG Bulletin*, *70*(3), 239-262.

Wermund, E. G., & Jenkins Jr, W. A. (1969). Late Pennsylvanian Shelf in North-Central Texas: ABSTRACT. *AAPG Bulletin*, 53(3), 749-749.

Wetzel, A. and Bromley, R.G. 1994. *Phycosiphon incertum* revisited: *Anconichnus horizontalis* is junior subjective synonym. *Journal of Paleontology*, 68:1396-1402.

Wilde, G. L. (1990). Practical fusulinid zonation: The species concept; with Permian basin emphasis: West Texas Geological Society. *Bulletin*, *29*(7), 5-13.

Yancey, T. E. (1991). Controls on carbonate and siliciclastic sediment deposition on a mixed carbonate–siliciclastic shelf (Pennsylvanian Eastern Shelf of north Texas). *Sedimentary Modeling: Computer Simulations and Methods for Improved Parameter Definition: Kansas Geological Survey, Bulletin*, *233*, 263-272

Curriculum Vitae

Robert Murphy
murphyinator@gmail.com

Education

Indiana University, Bloomington, IN 2015
Master of Science in Geoscience GPA 4.0

- Masters Thesis: Core Study, High Resolution Facies Model, and Integrated Reservoir Characterization of the Upper Wolfcamp Shale and Dean Sandstone, Midland Basin, TX

University of Texas Arlington, Arlington, TX 1997
Bachelor of Science in Geology GPA 3.4

- Earth Science Scholarship Recipient, Society of Independent Professional Earth Scientists Foundation, 1997

AAPG Education Conference Short Courses, 2012-2013

- Well Log Analysis, 5 day course
- Geologic Interpretation of Seismic Data
- Formation Evaluation of Thinly Bedded Reservoirs
- Exploring for Stratigraphic Traps Using Multi-well Pressure/Depth Plots

ESRI Short Courses, 2010

- ARCGIS Desktop
- ARCGIS Spatial Analyst

Employment History

Geoscience Intern
Employer: Pioneer Natural Resources**,** Irving, Texas 08/2014-11/2014

Research Assistant
Employer: Indiana University Shale Research Lab**,** Bloomington, IN
08/2011-05/2014

Geoscience Intern
Employer: Chevron Corporation, Bakersfield, California 04/2013-8/2013